Journal of Cleaner Production 426 (2023) 139203

Contents lists available at ScienceDirect

Journal of Cleaner Production

journal homepage: www.elsevier.com/locate/jclepro

# Solar-assisted photodegradation of pesticides over pellet-shaped $TiO_2$-kaolin catalytic macrocomposites at semi-pilot-plant scale: Elucidation of photo-mechanisms and water matrix effect

K. Jiménez-Bautista [a], A. Gascó [a], D.R. Ramos [b], E. Palomo [c], V. Muelas-Ramos [a], M. Canle [b], D. Hermosilla [a], A. Bahamonde [c,*]

[a] Department of Forest and Environmental Engineering and Management, Universidad Politécnica de Madrid, Escuela Técnica Superior de Ingeniería de Montes, Forestal y del Medio Natural, C/ José Antonio Novais 10, 28040, Madrid, Spain
[b] React! Group, Faculty of Sciences & CICA, Universidade da Coruña, E-15071, A Coruña, Spain
[c] Instituto de Catálisis y Petroleoquímica, ICP - CSIC, C/ Marie Curie 2, 28049, Madrid, Spain

ARTICLE INFO

Handling Editor: Jin-Kuk Kim

*Keywords:*
Immobilized catalysts
Solar photoreactors
Solar raceway
Real water matrix
Scavengers
Reactive species

ABSTRACT

The behavior of novel pellet-shaped bulky titania-kaolin photocatalysts is herein evaluated for its application in the solar-assisted photocatalytic treatment of a bio-recalcitrant pesticide mix (imidacloprid, pyrimethanil and methomyl) in solar lab-scale and semi-pilot scale raceway pond photoreactors. The photocatalyst consists of 1 cm long titania-kaolin macro-composites that combine some advantages of both nanoparticulate and supported catalysts without being either. This opening the opportunity to extend the use of this photocatalyst to complex wastewater effluents. In addition, their stability and reusability potential was also evaluated, and reactive species leading to the solar-degradation of each pesticide were also identified using radical scavengers. Total removal of pesticides (2 mg $L^{-1}$ each) with an optimal pellets dosage of 34.8 g $L^{-1}$ was addressed, whether in ultrapure water (180–270 min of solar irradiation) or in two basic pH Municipal Wastewater Treatment Plant (MWWTP) effluents (≤300 min of solar irradiation) where methomyl was always the most recalcitrant pesticide. Lower Total Organic Carbon (TOC) removal (≈53–56%) was also found under the effect of these complex MWWTP effluents than in ultrapure water (>60%). Those results are very promising when comparing to the almost negligible TOC removal achieved with the Titania powder under basic MWWTP effluents due to the strong effect of particle aggregation. Very good photocatalyst stability and durability was shown along three consecutive cycles after applying a low-cost recovery protocol consisting of several washing and drying cycles without addressing a significant photoefficiency loss (TOC≈60-56%). The application of scavengers revealed that hydroxyl radical generated from photoinduced holes was the dominant species in the degradation of pyrimethanil and methomyl whereas reactive oxygen species formed from conduction band electrons were mainly involved in the photo-oxidation of imidacloprid.

## 1. Introduction

Access to safe drinking water and water sanitation are essential human rights, as recognized by the United Nations General Assembly in 2010 and 2015, (United Nations, Unwater), and water is a key resource to ensure human well-being. The responsible use and proper treatment of water resources are crucial to ensure its availability in quantity and quality for future generations. Among human activities, agriculture globally accounts for the largest amount of annual water withdrawal worldwide (Li et al., 2020). As a consequence of this intensive water use, many pollutants, such as pesticides, growth hormones or endocrine disruptors, eventually end up in natural water bodies (Canle and Antão-Geraldes, 2023) and, of course, are present in different types of wastewater (Barbosa et al., 2016). Many of these organic pollutants that are toxic at very low concentration levels are difficult to degrade by conventional biological treatments and have been classified as contaminants of emerging concern (CECs) or priority pollutants (Muelas-Ramos et al., 2021). Water pollution by pesticides, synthetic products that do not exist in nature but widely used in agriculture, is a major environmental problem due to their potential toxicity and

* Corresponding author.
*E-mail address:* abahamonde@icp.csic.es (A. Bahamonde).

https://doi.org/10.1016/j.jclepro.2023.139203
Received 12 July 2023; Received in revised form 28 September 2023; Accepted 4 October 2023
Available online 6 October 2023

bioaccumulation, since the presence of pesticides in water can have adverse effects on human health and ecosystem equilibrium.

Advanced Oxidation Processes (AOPs) are promising treatment technologies that have been proven successful in efficiently remove bio-recalcitrant CECs from water (Sánchez et al. 2022, 2023). Among the available AOPs, semiconductor-mediated solar photocatalytic processes have several advantages over traditional wastewater treatment technologies. They are economical because they operate under mild conditions of both pressure and temperature, and the use an affordable and widely available semiconductor as the $TiO_2$-based catalytic composite used here, and solar radiation to generate the reactive species that degrade bio-recalcitrant compounds into harmless products (García--Muñoz et al., 2014; Malato Rodríguez et al., 2004). The key pathway for the generation of reactive species is based on the promotion of an $e^-$ from the valence band to the conduction band (Figure SI1); forming an electron-hole pair ($e^-_{CB}/h^+$) (Canle et al., 2012). The energy required to promote this $e^-$ corresponds to the bandgap (BG) and depends on the semiconductor properties. The anatase and brookite phases of $TiO_2$ have a BG ≈ 3.2 eV, while the rutile phase has a BG ≈ 3.0 eV (Kumar and Devi, 2011), which correspond to the UV radiation of the solar spectrum (Ibhadon and Fitzpatrick, 2013). The generated positive holes can react with water molecules producing hydroxyl radicals ($HO^\bullet$), and unpaired $e^-$ can react with oxygen molecules to produce other reactive oxygen species (ROS) (Gaya and Abdullah, 2008).

Processes based on $TiO_2$-based usually rely on micro- or nano-materials, which have an extremely high surface-to-volume ratio and therefore very high catalytic activity. However, it also implies the need for a further step of microfiltration to recover the used catalyst after the photocatalytic treatment. In addition, powder titania agglomerates under basic pH conditions, which significantly reduces its photo-efficiency. In this sense, the development of supported titania catalysts can overcome this problem. The application of immobilized catalysts provides a cost-efficient solution for wastewater treatment because the recovery of the catalyst to be reused is easier, faster and cheaper (Bagheri et al., 2014). The immobilization of nano-sized photocatalysts can eliminate the costly or even impracticable post-treatment recovery of the already used photocatalysts in large-scale operations. Moreover, supported titania catalysts do not undergo aggregation. Therefore, immobilized photocatalysts are widely accepted because they eliminate the need for expensive separation processes (Evgenidou et al., 2023). To this end, the anchoring of photocatalyst particles to larger, easily removable materials has been the subject of many excellent studies. As a result, researchers have coated a wide variety of surfaces such as quartz, glass, polymers, minerals, plant fibers, fly ash, vycor glass, polyethylene sheets, ceramic membranes, monoliths, glass slides, glass wool, anodized iron, optical fibers, Raschig rings, metals, clay and ceramics, thin films, reactor walls, etc. (Zhu et al., 2023; Silva et al., 2023; Park et al., 2022; and Deng et al., 2023).

However, immobilized catalysts generally have a lower surface-to-volume ratio than powder catalysts, which usually reduce their photo-efficiency and the degradation kinetics of the treatment process (Jiménez-Tototzintle et al., 2015; Dijkstra et al., 2001). The most important factor governing the efficiency of photocatalytic degradation is the minimization of the $e^-_{CB}/h^+$ pair recombination; therefore, it is necessary to maximize the rate of interfacial suitable molecules for $e^-_{CB}$ and $h^+$ trapping, since the photodegradation process exclusively takes place on the surface of the catalyst (Malato et al., 2009) or at a very short distance where $HO^\bullet$ could migrate (Sun et al., 1994). In addition, the frailty of photocatalytic coatings must be considered: immobilization is often weak due to poor attachment of the catalyst to the support, resulting in reduced activity in subsequent uses, and loose particles from the catalytic film can also contaminate the water (Razak et al., 2014; Ramos et al., 2021; Teixeira et al., 2016).

A novel bulky composite that does not contain any detachable film has been recently developed (Aguilar et al., 2023a). In this homogeneous composite of an Ecuadorian clay and $TiO_2$, the clay not just served as a support for the semiconductor, but also influenced its properties. The recovery and reuse of this pellet-shaped catalyst was very easy due to its large size. In addition, the bulk and surface compositions are the same, so its mechanical strength is less important than that of other immobilized photocatalysts, since the abrasion of the surface or the breakage of the pellets produces a new catalytic surface. Furthermore, the leaching of $TiO_2$ with use was almost negligible (Aguilar et al., 2023b), thus avoiding the addition of toxicity to the treated water. This material was shown to have good photocatalytic activity in the degradation of phenol (Aguilar *et al.*, 2023) and the inactivation of two bacterial species (Aguilar et al., 2023b). It has also been used as a tertiary treatment in a pilot-scale study to successfully remove nine persistent pollutants (Sánchez et al., 2022) and several pathogens (Sánchez, M.; 2021) from the effluent of a system comprising a hybrid digester and a subsurface vertical flow constructed wetland. A very similar catalyst was used in the present study, but a different clay, kaolin, was used to prepare the macro-composites. Kaolin, also known as china clay, is a naturally occurring white clay mineral composed primarily of the mineral kaolinite, a hydrated aluminum silicate with the chemical formula $Al_2Si_2O_5(OH)_4$. It is found in various regions of the world and has been used for centuries in a wide range of applications due to its unique properties. In this study, it was chosen because of the proximity to the largest European source of kaolin and, in particular, because of its high aluminum content.

On the other hand, and although the photodegradation mechanism of many individual pollutants along the photocatalytic process has been extensively reported, particularly for pesticides (Luna-Sanguino et al., 2019; Nitoi et al., 2013; Tolosana-Moranchel et al., 2017, 2020; Topalov et al., 2001; Villajos et al., 2021), the role of each pollutant contained in a complex effluent has not yet been fully elucidated in solar-assisted photodegradation, and studies with cocktails of substances are limited.

Therefore, the main goal of this paper has involved the development of a tertiary treatment using using $TiO_2$-based photocatalytic macro-composites for the solar-assisted photodegradation of organic micro-pollutants: a complex mixture of pesticides (imidacloprid, pyrimethanil and methomyl), which have been selected to cover a wide range of physicochemical and environmental properties, as justified in the experimental section, by solar-assisted heterogeneous photocatalysis. The behavior of this $TiO_2$-kaolin composite catalyst under the influence of different water matrices, such as an ultrapure water or a membrane bioreactor (MBR) effluent from a municipal wastewater treatment plant (MWWTP) was studied. For this purpose, the performance of different types of solar photoreactors was also evaluated, with the aim of providing further insights into the application of this type of catalysts in the treatment of real complex effluents at solar semi-pilot plant scale.

In addition, the stability and reusability of the used photocatalyst after its application in consecutive treatment cycles under the effect of different water matrices was also evaluated. This issue is of key importance for the economic and environmental evaluation of the applicability of photocatalytic processes for large-scale wastewater treatment. Finally, scavenging tests were performed in the presence of methanol, formic acid, and p-benzoquinone to induce quenching of $HO^\bullet$ radicals, photogenerated $h^+$, and $e^-$, with the aim of identifying the main reactive species involved in the solar degradation of the pesticide mixture studied here.

## 2. Experimental

### 2.1. Chemicals

The three pesticides selected for treatment were methomyl (99.5% purity), imidacloprid (99.7%), both supplied by Aragonesas Agro S.A., and pyrimethanil (98.2%), supplied by AgroEvo. Methomyl is a broad-spectrum carbamate insecticide used to control a variety of foliar and soil-borne insects; it is highly soluble in water, but it is not usually

persistent in soil or water systems, although it exhibits high overall toxicity (to flora, fauna, and human health). Imidacloprid is a chloronicotinic insecticide used to control sucking and soil insects, as well as for use on pets; it is highly soluble, mobile and persistent in water and soil, and has a high general toxicity. Pyrimethanil is an anilinopyrimidine fungicide that inhibits methionine synthesis, and has been used to control fungal pathogens on fruits, vegetables and ornamentals, with moderate persistence in soil and intermediate ecotoxicity. The properties of these contaminants, including their chemical structure and environmental persistence in terms of their estimated half-life in plants, which has been described as less variable than in soils, are summarized in Table SI1 (Agriculture & Environmental Research Unit, 2023; Fantke et al., 2014).

The catalyst was prepared with commercial $TiO_2$ (Degussa Aeroxide P25) and natural unrefined kaolin (provided by CAVISA, Ref. GF40M). Methanol (pure) was purchased from Scharlab, formic acid (85%) from Sigma-Aldrich and p-benzoquinone (pure) from Fluka. HPLC-grade orthophosphoric acid, methanol, and acetonitrile to perform chromatographic analyses were supplied by Scharlab. Milli-Q Type 1 water was used to prepare all solutions.

### 2.2. Preparation of the pellet-shaped titania-kaolin catalytic macrocomposites

The preparation of the bulky $TiO_2$-kaolin catalyst was carried out according to a patented method (Ramos et al., 2020) that was chosen for its extreme simplicity to provide an efficient and stable immobilized photocatalyst in the reaction medium (Aguilar et al., 2023a). This procedure involved first thoroughly mixing dry powdered $TiO_2$ (90% by weight) and kaolin (10% by weight); then, adding water dropwise to form a paste that was extruded with a syringe (2.4 mm inner diameter-tip) into long cylinders on aluminum foil. After drying at 90 °C for 12 h, the rolls were broken into smaller pellets approximately 1 cm long and then calcined in a muffle at 600 °C for 3 h with a heating ramp of 5 °C·min$^{-1}$. After cooling to room temperature, these composite pellets were rinsed with water to remove loose particles and dried again at 90 °C (Figure SI1).

### 2.3. Characterization of the catalyst

Both the starting materials and the catalyst prepared from them were fully characterized. The chemical composition of P25 $TiO_2$ and natural kaolin was measured by X-ray fluorescence (XRF) in a Bruker S4 Pioneer XRF spectrometer, and their granulometry was determined by laser light scattering in a Micromeritics Saturn DigiSizer II instrument. The density of these precursors was obtained using a Micromeritics Accupyc 1340 He pycnometer.

Powder X-ray diffraction (XRD) patterns were performed on a PANalytical X'Pert PRO polycrystal X-ray diffractometer using nickel-filtered Cu Kα radiation and an ultrafast X'Celerator detector, while the precursors were analyzed in a Bruker D4 Endeavor instrument. Anatase and rutile crystalline phases ratios were determined by the Spurr and Myers method (Spurr and Myers, 1957), and average crystallite sizes were calculated by means of the Scherrer equation (Jenkins and Zinder, 1996).

The BET surface area and the microporous and mesoporous structure of the catalytic pellets and their precursors were analyzed from the $N_2$ adsorption-desorption isotherms at −196 °C obtained with a Micromeritics ASAP 2420 (pellet catalyst) and a Micromeritics TriStar II Plus (precursors) on samples previously outgassed overnight at 140 °C to a residual pressure of $<10^{-4}$ Pa. Mercury intrusion porosimetry (MIP) was used to determine the macropore volume of the catalyst using a Micromeritics AutoPore IV 9510 device. The total pore volume was evaluated by combining both techniques.

The surface and cross-section of the catalytic pellets were studied by scanning electron microscopy (SEM) coupled with energy-dispersive X-ray spectroscopy (EDS) using a JEOL 6400 JSM microscope, both taking micrographs images and analyzing the chemical composition of several areas.

### 2.4. Solar photocatalytic treatment

All solar photodegradation runs were carried out under the following initial operating conditions: atmospheric pressure, ambient temperature, natural pH, the corresponding initial pesticide concentration considered for each evaluated photoreactor (namely, 2 or 5 mg L$^{-1}$ of each pesticide in the mix), and different doses of $TiO_2$-kaolin pellets. 20, 30, 40, 60, and 70 g L$^{-1}$ of catalytic pellets were used in conical solar batch reactors, while 20 and 34.8 g L$^{-1}$ were used for the semi-pilot solar raceway pond reactor (RPR).

The influence of three different water matrices on the photodegradation of this pesticide mixture was evaluated using MilliQ-ultrapure water (UW) and two different final MBR-treated effluent streams from a MWWTP located in Garray (Soria, Spain) with contrasting characteristics (E1 and E2), whose physicochemical properties are summarized in Table 1. E2 contains about 10–15% higher concentration of each ion, therefore its conductivity and total dissolved solids content are also higher, and its pH value is more basic (8.1–8.6 for E2 vs. 7.9–8.1 for E1).

Two different solar photocatalytic reactors were used to investigate the solar photodegradation of the mixture of three selected pesticides with the recently developed titania-kaolin macrocomposite, namely: laboratory-scale conical batch reactors (1L Pyrex Erlenmeyer flasks), and a semi-pilot-scale RPR (Figure SI2). First, catalyst dosage and solar photomechanism elucidation were investigated in 1 L Pyrex Erlenmeyer flasks containing 100 mL of the pesticide mixture, which served as conical solar batch reactors, providing an inclined wall to sunlight along the experiments.

In addition, a pilot-scale polypropylene solar raceway pond reactor (RPR) was used to analyze the photocatalytic activity of the $TiO_2$-kaolin catalytic material in the solar degradation of the selected pesticide mixture under the effect of different water matrices. This 600 mm long and 300 mm wide RPR consists of an open canal through which water is circulated by the action of a paddle wheel connected to a 9 rpm motor (Figure SI2). It thus provides an illuminated area of ≈0.18 m$^2$, while the water depth can be regulated to adjust the total solar radiation incident on the aqueous volume. For these runs, 4 L of wastewater was added to the RPR, resulting in a water height of ≈2.25–2.5 cm.

Photocatalytic tests were performed outdoors at ICP-CSIC, at 40° N latitude (Madrid, Spain). The incident irradiance was measured with a CUV3 Kipp & Zonen broadband UV radiometer (285–400 nm) placed in

**Table 1**
Physicochemical parameters of the three studied water matrices.

| Parameter | Ultrapure Water (UW) | MWWTP Effluent 1 (E1) | MWWTP Effluent 2 (E2) |
|---|---|---|---|
| pH | 6.5 | 7.9–8.1 | 8.1–8.6 |
| **TOC** (mg·L$^{-1}$) | < 0.2 | < 4.0 ± 0.01 | < 5.0 ± 0.01 |
| **Conductivity** (mS·cm$^{-1}$) | – | 1.9 ± 0.2 | 2.1 ± 0.2 |
| **$CO_3^{2-}$** (mg·L$^{-1}$) | n. d. | 420 ± 30 | 470 ± 30 |
| **$Ca^{2+}$** (mg·L$^{-1}$) | n. d. | 130 ± 10 | 149 ± 13 |
| **$Mg^{2+}$** (mg·L$^{-1}$) | n. d. | 48.0 ± 7.0 | 53.0 ± 3.0 |
| **$K^+$** (mg·L$^{-1}$) | n. d. | 42.0 ± 0.8 | 47.0 ± 1.0 |
| **$Na^+$** (mg·L$^{-1}$) | n. d. | 258 ± 50 | 287 ± 56 |
| **$Cl^-$** (mg·L$^{-1}$) | n. d. | 194 ± 60 | 215.6 ± 70 |
| **$NO_3^-$** (mg·L$^{-1}$) | n. d. | 15.0 ± 1.0 | 17.0 ± 1.1 |
| **$NO_2^-$** (mg·L$^{-1}$) | n. d. | < 0.25 | < 0.30 |
| **$SO_4^{2-}$** (mg·L$^{-1}$) | n. d. | 338 ± 22 | 375 ± 24 |
| **$PO_4^{3-}$** (mg·L$^{-1}$) | n. d. | 3.8 ± 0.7 | 4.3 ± 0.7 |
| **$NH_4^+$** | n. d. | n. d | n. d. |
| **Total dissolved solids** (g·L$^{-1}$) | n. d. | 0.09 ± 0.01 | 1.00 ± 0.01 |

MWWTP = Municipal WasteWater Treatment Plant.

the same orientation of the RPR, resulting in an average irradiance of 30.2 W $m^{-2}$. In addition, complementary experiments were performed with the well-known commercial P25 $TiO_2$ powder catalyst to provide a reference for the results obtained in the RPR.

To determine the efficiency of both solar photoreactors, a normalization process of the reaction time was performed to standardize the solar irradiance (Guillard et al., 2003; Prieto-Rodriguez et al., 2012), namely:

$$E_{UV,n} = E_{UV,n-1} + \Delta t_n \cdot \overline{UV}_n \cdot \frac{S_p}{V_{TOT}} \quad (1)$$

$$\Delta t_n = t_n - t_{n-1} \quad (2)$$

where $t_n$ is the experimental time at which each sample was taken, $S_p$ is the illuminated surface of the reactor, $V_{TOT}$ is the total volume of water treated, $\overline{UV}_n$ is the average radiation measured during this period, and finally, $E_{UV,n}$ is the total energy collected in the photoreactor. To simplify the calculation of the kinetic constants, it can be assumed that the average solar UV irradiance at noon (±2 h) on a fully sunny day is approximately 30 W $m^{-2}$ (Malato et al., 2009; Adan et al., 2009). Thus, the reaction time can be expressed in the following way:

$$t_{30W,n} = t_{30w,n-1} + \Delta t_n \cdot \frac{\overline{UV}_n}{30} \cdot \frac{S_p}{V_{TOT}} \quad (3)$$

Preliminary adsorption tests were carried out in dark conditions. Although clays are usually very good adsorbents, these experiments showed a negligible amount of pesticides adsorbed on these catalyst $TiO_2$-kaolin pellets (<1%), in agreement with the data obtained with the pellets prepared with Ecuadorian clay (Aguilar et al., 2023b). Thus, no dark pre-adsorption step was required before performing the solar photocatalytic treatment experiments. All assays were performed in triplicate. The calculated standard errors were always smaller than 5–10%. Therefore, for graphical clarity, error bars have not been included in the figures.

High performance liquid chromatography, HPLC (Azura, by Knauer), with photodiode array detection was used to identify and quantify pesticide concentrations along the treatment. The total organic carbon (TOC) content was also monitored in the reaction medium withdrawing samples at different irradiation times, which were measured with a TOC-VCSH/CSN Shimadzu analyzer.

#### 2.4.1. Evaluation of catalyst stability

The used titania-kaolin pellets in the photocatalytic treatments in the semi-pilot plant-scale solar RPR were recovered and reused again for four consecutive runs of 360 min of solar irradiation each, under optimized reaction conditions. The recovery procedure consisted of a low-cost process involving three tap water plus three ultrapure water rinses, followed by exposure of the catalytic pellets to sunlight in water for 8 h, and finally drying in an oven at 90 °C for 12 h. In addition, the Ti content was measured by inductively coupled plasma atomic emission spectroscopy (ICP-AES, PlasmaQuant® PQ 9000, Analytik Jena) at the end of each experiment to determine whether $TiO_2$ was leached into the solution.

#### 2.4.2. Study of the solar photodegradation mechanism

Finally, the main pathways of the pesticide photodegradation mechanism were elucidated by the effect of three scavengers in conical solar batch photoreactors: methanol (100 mM) as $HO^{\bullet}$ scavenger, p-benzoquinone (10 mM) to scavenge superoxide ($O_2^{\bullet-}$) formed from conduction band electrons ($e_{CB}^-$), and formic acid (5 mM) to quench photogenerated holes ($h^+$). The initial operating conditions were the following: a catalytic $TiO_2$-kaolin macrocomposite dosage of 20 g $L^{-1}$ and an initial concentration of 5 mg $L^{-1}$ of each pesticide in ultrapure water, corresponding to a TOC content of 10 mg $L^{-1}$.

## 3. Results and discussion

### 3.1. Characterization of the pellet-shaped titania-kaolin catalytic macrocomposites

P25 $TiO_2$ and natural kaolin were mixed and calcined to produce a composite with photocatalytic activity. Therefore, the resulting composite retains some of the physicochemical properties of the original materials, which have also been characterized (Table 2).

As already observed with similar catalysts prepared with titania and another type of clay (Aguilar et al., 2023a), their chemical composition results from the addition of those of the raw semiconductor and clay in their corresponding ratios, with some small differences due to minor soluble salts or thermally unstable compounds, such as $P_2O_5$, which reacts with water to form $HPO_3$ and evaporates during calcination. The photocatalytic activity of rutile is much lower than that of anatase, and their ratio is optimized in P25 $TiO_2$, but a mineral phase transition occurs in $TiO_2$ at high calcination temperatures. However, the high Al content in kaolin can inhibit the transformation of anatase to rutile (Hanaor and Sorrell, 2011), which occurs from 600 °C at atmospheric pressure. In this case, and according to the XRD patterns of raw kaolin and P25 $TiO_2$ powders and the catalyst pellets (Fig. 1), the peaks of the latter result from the approximate combination of those observed in the precursors, with the intensities determined by their relative weights in the catalyst composition. In fact, the anatase/rutile ratio in the catalyst pellets (75/25) is almost the same as in untreated P25 $TiO_2$ (76/24), indicating that the kaolin has quite successfully inhibited the anatase to rutile phase transition during calcination. This effect was also observed with the pellets composed of titania and Ecuadorian clay (Aguilar et al., 2023a). The BET surface area increases slightly to 72.5 $m^2$ $g^{-1}$ when the precursors are mixed with water, extruded and mildly calcined.

The density of kaolin is significantly lower than that of P25 $TiO_2$ and its granulometry is coarser. Therefore, on average, the titania-kaolin catalyst consists of some larger clay particles, about 15% by volume, surrounded by smaller $TiO_2$ particles. The pellets exhibit an irregular surface under the electron microscope (Fig. 2A and B), with titania and kaolin homogeneously distributed at the surface (Fig. 2C) and throughout the pellet (Fig. 2D) according to EDS maps, indicating that the surface and bulk compositions are the same.

### 3.2. Photocatalytic activity of the pellet-shaped titania-kaolin catalytic macrocomposites in conical solar batch reactors

The optimization of the catalyst dosage was first carried out in conical solar batch photoreactors to study its photocatalytic performance in the solar photodegradation of the selected pesticide mixture (see Fig. 3). The corresponding degradation curves were fitted to pseudo-first order kinetic constants, considering that a modified

**Table 2**
Physicochemical properties of the raw materials employed for the preparation of pellet-shaped immobilized titania-kaolin catalyst.

| Material | Chemical composition (%) | | | | | |
|---|---|---|---|---|---|---|
| **P25 $TiO_2$** | $TiO_2$ | Cl | CuO | | | |
| | 99.8 | 0.12 | 0.017 | | | |
| **Kaolin** | $SiO_2$ | $Al_2O_3$ | $K_2O$ | $Fe_2O_3$ | MgO | $TiO_2$ |
| | 52.4 | 42.2 | 3.0 | 1.6 | 0.23 | 0.17 |
| | $P_2O_5$ | CaO | $Rb_2O$ | ZnO | MnO | |
| | 0.084 | 0.047 | 0.030 | 0.013 | 0.013 | |

| | Mineral phases | | | Density ($g \cdot mL^{-1}$) | Mean particle size (μm) | BET surface area ($m^2 \cdot g^{-1}$) |
|---|---|---|---|---|---|---|
| **P25 $TiO_2$** | Anatase | Rutile | | 4.38 | 6.02 | 50.92 |
| **Kaolin** | Kaolinite | Quartz | Muscovite | 2.66 | 23.6 | 11.84 |

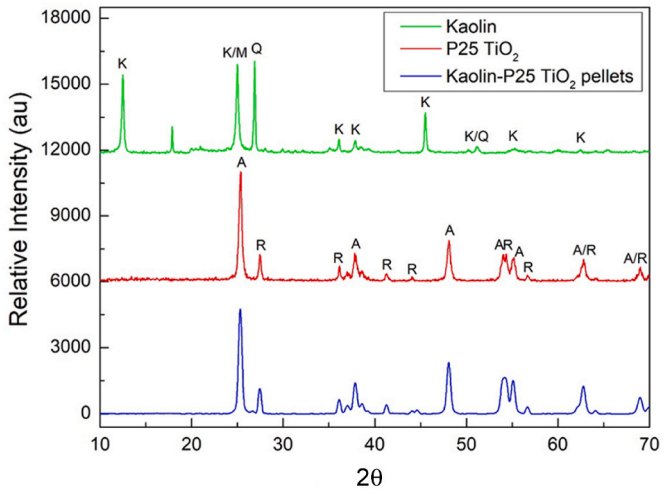


**Fig. 1.** XRD patterns of powdered kaolin and commercial Aeroxide P25 $TiO_2$, and the evaluated pellet-shaped immobilized titania-kaolin catalyst. Identified mineral phases are indicated: kaolinite (K), quartz (Q), muscovite (M), anatase (A), and rutile (R).

Langmuir-Hinshelwood kinetic model adequately describes the kinetics of this heterogeneous photocatalytic process (Malato et al., 2009; Toepfer et al., 2006); thus allowing to calculate the corresponding apparent kinetic constant, $k_{pesticide}$, for each pesticide (see Table 3). High coefficients of determination ($r^2$ = 0.920–0.998) were obtained in all cases. In addition, the evolution of TOC content was monitored during 360 min of solar irradiation and TOC conversions ($X_{TOC,}$ %) were calculated to determine the optimal catalyst dosage for solar photodegradation of the pesticide mixture (Table 3).

Although higher photodegradation rates were obtained by increasing the catalyst dosage from 20 up to 70 g $L^{-1}$, TOC conversions did not significantly improve at higher catalyst dosages with an average TOC removal of 73.3% (Table 3). Therefore, it seems reasonable to assume a compromise between catalyst dosage and TOC removal to avoid an excessive amount of catalyst that would increase both the economic cost and environmental impact of the proposed solar photocatalytic treatment. Therefore, considering the obtained results, 20 g $L^{-1}$ was selected as the compromise optimal dosage of titania-kaolin catalyst to perform the photocatalytic treatment of the target pesticide mixture in these photoreactors.

In addition, higher pseudo-first order kinetic constants were always obtained for the degradation of imidacloprid and pyrimethanil, while lower values were generally observed for methomyl (Fig. 3 and Table 3). In fact, despite its high toxicity, methomyl is an aliphatic compound (Table SI1) with low environmental persistence because this type of substance is more easily biodegraded in the environment than aromatic ones such as pyrimethanil and imidacloprid. Correspondingly, aromatic substances are easier to oxidize opening the aromatic ring than linear open chain molecules (Hermosilla et al., 2009; Pignatello et al., 2006) despite their molecular weight or functional group content because of the rather easy opening of aromatic rings by oxidation. This was supported by the similar degradation results obtained for pyrimethanil and imidacloprid. Faster degradation of imidacloprid than pyrimethanil could be attributed to a first dechlorination step that modifies the molecule before promoting ring opening, as has been previously reported for other chlorinated aromatic pollutants.

On the other hand, the influence of two initial pesticide concentrations (2 and 5 mg $L^{-1}$ of each pesticide) on the photocatalytic degradation was also evaluated. Although the photodegradation rates of the pesticides did not improve when a lower concentration was tested, a significant ~3% increase in TOC reduction was observed (Table 3). Considering these results, 2 mg $L^{-1}$ of the initial pesticide concentration and 20 g $L^{-1}$ of the pellet dosage were selected as the operating conditions to evaluate the performance of this pellet-shaped titania-kaolin composite in the solar RPR pilot plant.

### 3.3. *Solar-assisted photodegradation of pesticides in a solar raceway pond reactor using the pellet-shaped titania-kaolin catalytic macrocomposites*

The post-treatment removal of fine particulate catalysts from treated wastewater represents a significant environmental and economic impact on the benefits that might otherwise be obtained from photocatalysis (Borges et al., 2016). In this context, the immobilization of photocatalysts implies the suppression of this costly recovery step, which is particularly useless when dealing with the treatment of natural or real wastewater effluents in large-scale operations.

Although compound parabolic collectors (CPC) are low-concentrating devices that have already been reported as a very photoefficient technology for industrial wastewater or tertiary treatment, they are still quite expensive (about 400 €·$m^{-2}$) (Fiorentino et al., 2019; Cabrera-Reina et al., 2021). So-called raceway pond reactors (RPRs) have recently been addressed as an alternative technology for application in the advanced treatment of urban wastewater, reducing the cost of other solar reactors, estimated at about 10 €·$m^{-2}$ (Carra et al., 2014; Soriano-Molina et al., 2019). Although CPCs have been reported to efficiently harvest light, they have a low ratio of treated water volume to

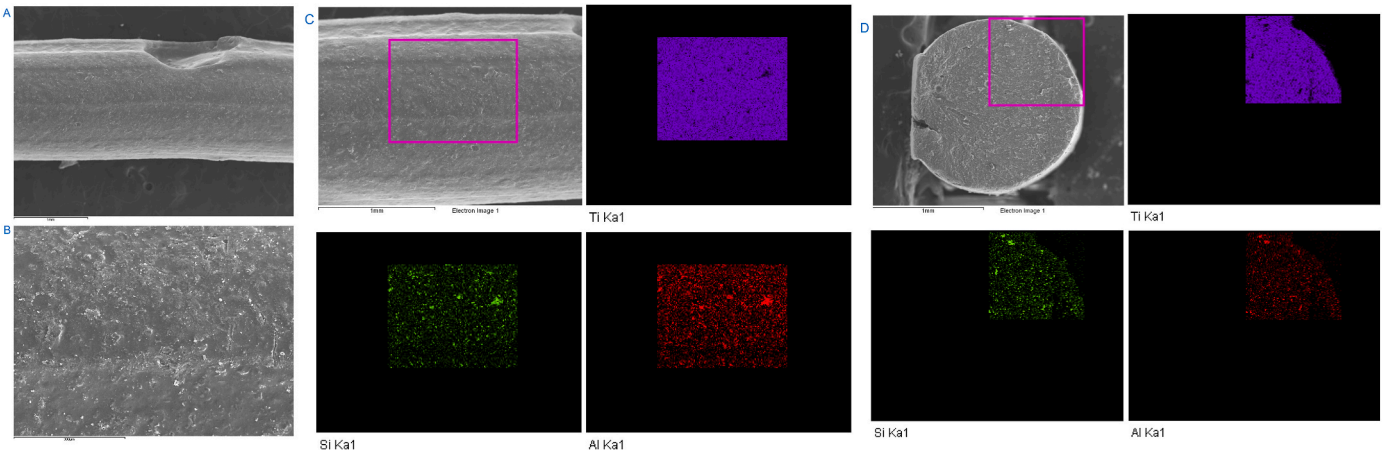


**Fig. 2.** SEM electron micrographs of the surface of $TiO_2$-kaolin catalytic pellets at different magnifications (A & B), and EDS maps showing the distribution of Ti, Si and Al at the surface (C) and in the cross section (D) of the catalytic pellets. Note: the colors used have no chemical meaning. (For interpretation of the references to color in this figure legend, the reader is referred to the Web version of this article.)

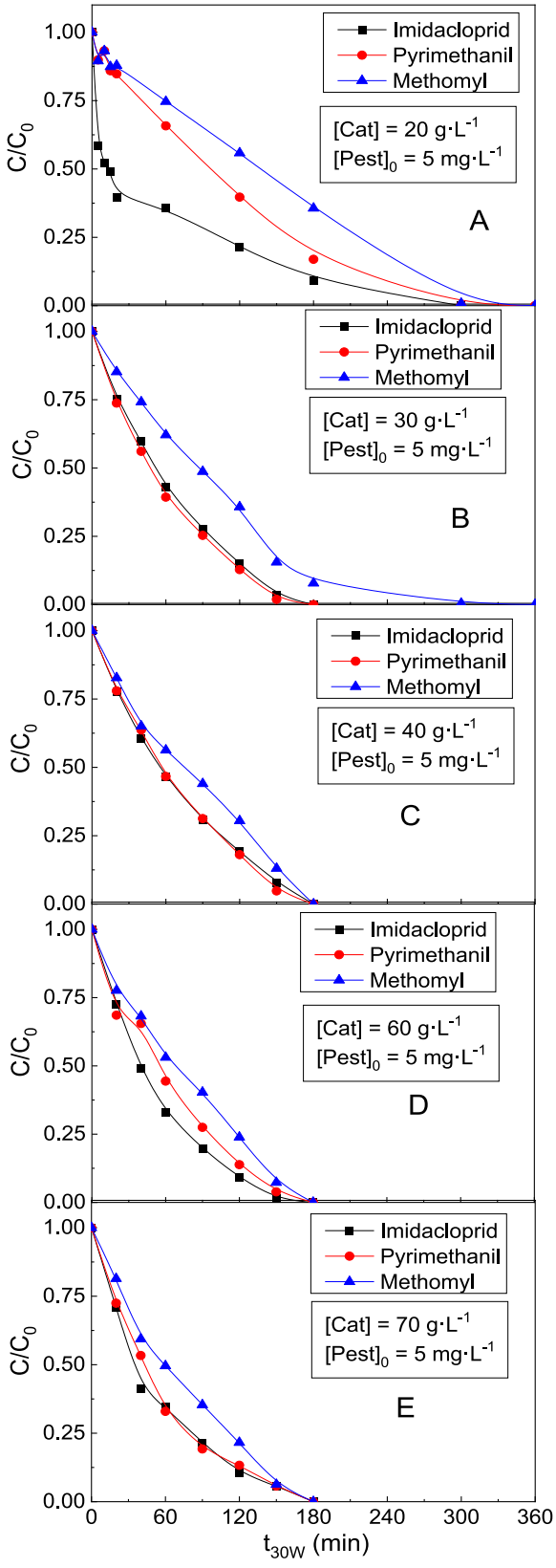


**Fig. 3.** Effect of catalytic pellets dosage on the evolution of photodegradation of pesticides mixed in ultrapure water in conical solar batch photoreactors: [catalyst] = (A) 20, (B) 30, (C) 40, (D) 60, and (E) 70 g $L^{-1}$.Imidacloprid (■), pyrimethanil (●), and methomyl (▲). Operating conditions: $[pesticides]_0$ = 5 mg $L^{-1}$ of each pesticide in the mixture, $[TOC]_0$ = 10 mg $L^{-1}$, ambient T and P.

illuminated area, whereas in RPRs the volume of wastewater can be easily adjusted, facilitating the optimization of operating conditions (De la Obra et al., 2017).

Preliminary studies have shown that powdered $TiO_2$ catalysts mix very well with the polluted effluent, with a very good fluid dynamic behavior along the tubular reactors of the solar CPC photoreactor, whereas the titania-kaolin catalytic material has some important operational problems because it does not remain stationary but flows through the CPC tubes. In addition, good mixing of the polluted effluent with the catalyst pellets was not achieved along the CPC tubes due to the accumulation of the pellets in the tube elbows. Therefore, pilot scale experiments were conducted in the solar RPR described above.

Fig. 4 and Table 4 summarize the results obtained for the photocatalytic treatment of the target pesticide mixture in UW using different dosages of catalyst pellets in the RPR. A significant increase in TOC removal (from 26.7% to 61.1%) and much faster pseudo-first order kinetic constants (3–6 times) were observed when the pellet-shaped catalyst dosage was increased from 20 to 34.8 g $L^{-1}$, which corresponds to the bottom of the solar RPR completely covered with pellets. At this optimized catalyst dosage, less than 250 min of solar irradiation was enough to achieve complete degradation of the pesticides; whereas only imidacloprid was completely removed after 390 min of solar irradiation when the 20.0 g $L^{-1}$ dosage of the pellet-shaped catalyst was used.

In addition, imidacloprid was degraded relatively faster than pyrimethanil, and methomyl was the most difficult to degrade. Furthermore, greater differences in degradability by solar photocatalysis were found among the pesticides at lower concentration (2 mg $L^{-1}$ of each pesticide). These results are consistent with those previously presented and discussed for conical solar batch photoreactors.

### *3.3.1. Stability evaluation of the pellet-shaped titania-kaolin catalytic macrocomposites*

Stability and reusability of the photocatalyst along consecutive uses are very relevant issues for the application of cost-effective immobilized catalysts in photocatalytic processes of real wastewater treatment on a large scale. Thus, the stability and reusability of these novel titania-kaolin catalytic macrocomposites were tested by performing four consecutive reuse cycles of 300 min of solar irradiation, photodegrading the pesticide mixture in ultrapure water matrix (UW) in the solar RPR. The catalyst pellets were recovered after each use and reused again after the very simple washing procedure described in the experimental section. A more complex washing process, using more efficient cleaning solutions, was discarded for two reasons: to keep the cost as low as possible and to propose a very green and sustainable treatment method that uses sunlight and avoids the use of chemicals other than for catalyst production.

The performance of the catalyst over these four cycles is shown in Fig. 5. Complete pesticide removal was achieved in 300–360 min of solar irradiation in the first three cycles. However, more than 390 min were required to remove methomyl in the last cycle (see Fig. 5A). Furthermore, the mineralization of organic matter was almost constant in the first and second treatment cycles of use (TOC removal ≈ 60–61%), while it slightly decreased in the third cycle (TOC removal = 56.0%) and the catalyst performance significantly worsened when the catalyst pellets were reused for the fourth round (TOC removal = 43.5%, see Fig. 5B). In short, a constant performance and adequate stability of these pellets has been demonstrated for at least three application cycles of 360 min of solar irradiation in the solar RPR.

The loss of catalytic activity could be well related to photocatalyst deactivation caused by different mechanical, thermal or even chemical factors. According to the ICP-AES measurements, $TiO_2$ was not leached from the catalytic pellets into the solution along the experiments performed, not even after several reuses, proving their excellent mechanical stability. Therefore, deactivation could be caused either by poisoning of the active sites on the surface with refractory, non-oxidizable by-

**Table 3**
Optimization of the catalytic pellets' dosage in the solar pesticide photodegradation under ultrapure water matrix in conical solar batch photoreactors.

| [Cat] ($g{\cdot}L^{-1}$) | $[Pest]_0$ ($mg{\cdot}L^{-1}$) | $X_{TOC}$ (%) | Pseudo first kinetic constants | | | | | |
|---|---|---|---|---|---|---|---|---|
| | | | $k_{Imidacloprid}$ ($min^{-1}$) | $r^2$ | $k_{Pyrimethanil}$ ($min^{-1}$) | $r^2$ | $k_{Methomyl}$ ($min^{-1}$) | $r^2$ |
| 20 | 2 | 76.4 ± 0.4 | 0.0105 | 0.920 | 0.0102 | 0.975 | 0.0053 | 0.980 |
| 20 | 5 | 73.2 ± 1.0 | 0.0111 | 0.979 | 0.0121 | 0.979 | 0.0073 | 0.967 |
| 30 | 5 | 66.0 ± 1.0 | 0.0156 | 0.992 | 0.0168 | 0.993 | 0.0113 | 0.925 |
| 40 | 5 | 74.0 ± 1.0 | 0.0137 | 0.998 | 0.0141 | 0.992 | 0.0096 | 0.995 |
| 60 | 5 | 75.6 ± 0.8 | 0.0198 | 0.995 | 0.0159 | 0.972 | 0.0114 | 0.983 |
| 70 | 5 | 77.6 ± 1.0 | 0.0187 | 0.993 | 0.0175 | 0.993 | 0.0125 | 0.993 |

[Cat] = catalytic pellets' dosage, $[Pest]_0$ = initial concentration of each pesticide in the mixture (imidacloprid, pyrimethanil and methomyl), $X_{TOC}$ (%) = Total Organic Carbon conversion in 300 min of solar irradiation.

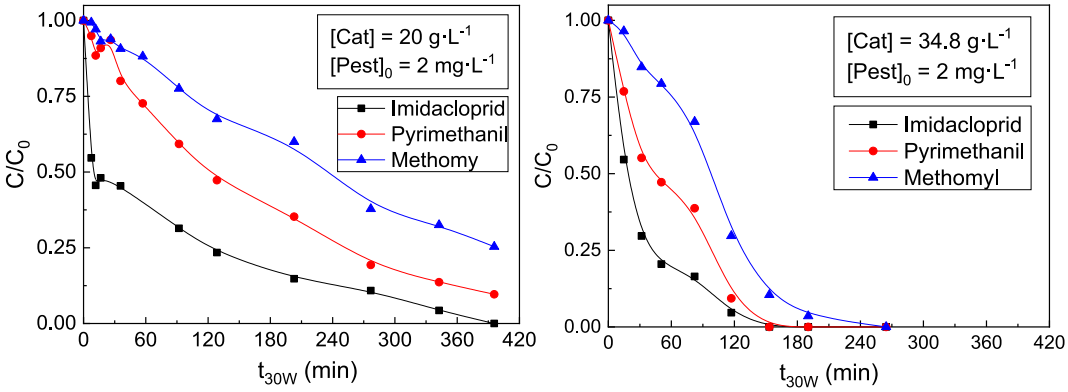


**Fig. 4.** Effect of catalytic pellets dosage on the evolution of the photodegradation of pesticides mixed in ultrapure water in the solar raceway pond reactor: [catalyst] = (A) 20 and (B) 34.8 g $L^{-1}$. Imidacloprid (■),pyrimethanil (●), and methomyl (▲). Operating conditions: $[pesticides]_0$ = 2 mg $L^{-1}$ of each pesticide in the mixture, $[TOC]_0$ = 4 mg $L^{-1}$, ambient T and P.

**Table 4**
Optimization of the catalytic pellets' dosage in the solar pesticide photodegradation under ultrapure water matrix in a solar RPR.

| [Cat] ($g{\cdot}L^{-1}$) | $[Pest]_0$ ($mg{\cdot}L^{-1}$) | $X_{TOC}$ (%) | Pseudo first kinetic constants | | | | | |
|---|---|---|---|---|---|---|---|---|
| | | | $k_{Imidacloprid}$ ($min^{-1}$) | $r^2$ | $k_{Pyrimethanil}$ ($min^{-1}$) | $r^2$ | $k_{Methomyl}$ ($min^{-1}$) | $r^2$ |
| 20.0 | 2 | 26.7 ± 0.7 | 0.0073 | 0.950 | 0.0058 | 0.994 | 0.0032 | 0.967 |
| 34.8 | 2 | 61.1 ± 1.0 | 0.0236 | 0.951 | 0.0180 | 0.900 | 0.0172 | 0.906 |

[Cat] = catalytic pellets dosage, $[Pest]_0$ = initial concentration of each pesticide in the mixture (imidacloprid, pyrimethanil and methomyl), $X_{TOC}$ (%) = Total Organic Carbon conversion in 300 min of solar irradiation.

products, or by clogging with fine particulate matter from the urban air of Madrid, where the experiments were performed. In particular, urban atmospheric particulate matter contains metals and polycyclic aromatic hydrocarbons (PAHs), among other chemicals (Jin et al., 2019), and, although PAHs can be removed by catalytic photodegradation (Misawa et al., 2020), deposited metals cannot be removed by this oxidation technology. Consequently, the deposition of these materials and reaction by-products on the surface of the catalyst pellets would have fouled and clogged them after four consecutive reuse cycles (Argly and Bartholomew, 2015; Kusworo et al., 2022; Ren et al., 2023).

To validate this hypothesis, the textural properties of the catalytic pellets were measured before their first use (fresh pellets), after their first use plus washing, and after their reuse in four consecutive cycles of solar RPR treatment of the pesticide mixture in UW. The obtained textural results are presented in Table 5, and the corresponding $N_2$-adsorption-desorption isotherms and pore size distributions are shown in Figure SI3. All these catalyst pellets exhibited type II isotherms according to the Brunauer-Deming-Deming-Teller (BDDT) classification (Figure SI3A), which are characteristic of low porosity materials (Rahman et al., 2021). In all cases, a type H1 hysteresis cycle was observed, which is usually associated with a narrow distribution of uniform pores. This is confirmed in Figure SI3B, where well-defined mesopores of about 44 nm width are shown in all cases. In general, the textural properties of the pellets (Table 5) are mainly governed by the mesoporosity (≈98.9%) and contain only a small percentage of macropores (≈1.21%). It can be emphasized that these catalytic pellets show a monomodal mesoporous size distribution (Figure SI3B) and their pore size does not change significantly when were used in four consecutive treatment cycles (Table 5). Although only slight differences were observed between fresh and washed pellets after one use and recovery cycle (Table 5), a significant loss of surface area (*ca.* 40% lower) and especially in mesopore volume (*ca.* 5% reduction) was found in the pellets that were reused four times.

The EDS analysis showed a significant reduction in the weight percentage of Ti at the surface of the reused pellets compared to the fresh ones (8.4% less), but this was accompanied by a similar decrease in the Si and Al values (11.5% less). Considering that no changes were observed in the XRD patterns of the used pellets (data not shown because no differences were obtained in comparison with the fresh pellets patterns shown in Fig. 1) and leaching of Ti was not detected, it is plausible

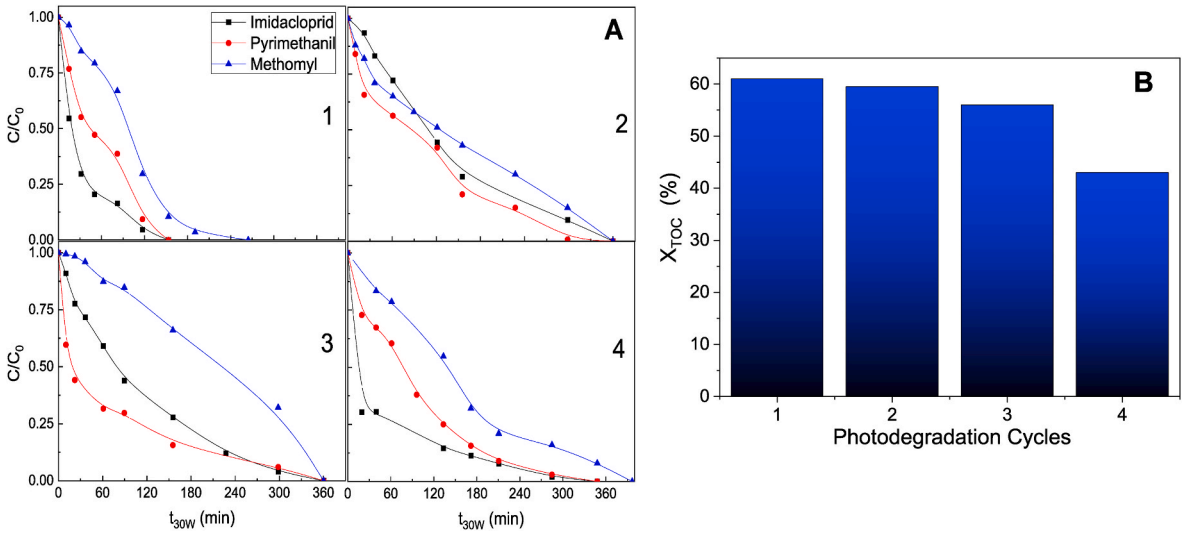


**Fig. 5.** (A) Evolution of pesticides photodegradation and (B) TOC conversion ($X_{TOC}$, %) along four consecutive cycles (300 min each) of the catalytic pellets in the solar raceway pond reactor under ultrapure water. Imidacloprid (■),pyrimethanil (●), and methomyl (▲). Operating conditions: [catalyst] = 34.8 g $L^{-1}$, $[pesticides]_0$ = 2 mg $L^{-1}$ of each pesticide in the mixture, $[TOC]_0$ = 4 mg $L^{-1}$, ambient T and P.

**Table 5**
Textural properties of fresh, used and washed once, and reused catalytic pellets along consecutive solar pesticide photodegradation cycles under ultrapure water (UW) or MWWTP Effluent 2 (E2‡) in a solar RPR.

| Catalyst | Water matrix | $S_{BET}$ ($m^2 \cdot g^{-1}$) | $V_{micropores}$ ($cm^3 \cdot g^{-1}$) | $V_{mesopores}$ ($cm^3 \cdot g^{-1}$) | $V_{Macropores}$ ($cm^3 \cdot g^{-1}$) | $V_{Total}$ ($cm^3 \cdot g^{-1}$) |
|---|---|---|---|---|---|---|
| Fresh Pellets | UW | 72.5 | 0.000 | 0.402 | 0.0048 | 0.407 |
| Washed Pellets | UW | 70.5 | 0.000 | 0.400 | 0.0039 | 0.404 |
| Reused Pellets | UW | 43.5 | 0.000 | 0.381 | 0.0022 | 0.383 |
| Reused Pellets | E2 | 37.6 | 0.000 | 0.348 | 0.0061 | 0.354 |

$[Pesticides]_0$ = 2 mg $L^{-1}$ of each pesticide (imidacloprid, pyrimethanil and methomyl), $[TOC]_0$ = 4 and 9 mg $L^{-1}$ ‡E2 water matrix characteristics in Table 1.

to conclude that their chemical structure should not have changed. Therefore, the mentioned deactivation phenomena observed after four reuse cycles could have been the result of fouling caused by the deposition of different substances, that clog the external surface of the catalyst, plugging pores and partially blocking its BET surface area, which then decreases in the used pellets (Table 5), and also reduces the amount of composite material (Ti, Si and Al) at the surface of the pellets. Unfortunately, the cleaning procedure used to regenerate the used pellets only worked for a couple of cycles. Furthermore, the sunlight regeneration step was performed in uncapped crystallizers, so while most of the organic matter was certainly photodegraded, additional particulate matter may have been deposited, contributing to fouling. Therefore, further research is currently in progress to increase the reusability of these catalyst pellets by developing a better cleaning protocol while keeping the cost low.

### 3.3.2. *Influence of the water matrix on the performance of the catalyst*

The performance of the catalytic macrocomposites in the treatment of pesticides by solar photocatalysis in the RPR was compared with that of the well-known commercial powdered P25 $TiO_2$ catalyst, which was used as reference. The latter showed a very different photoefficiency when UW and MWWTP effluents (E1 and E2, see Table 1) were used to prepare the pesticide mixture. The main results are summarized in Table SI2, and additional information showing the evolution of the treatment with P25 $TiO_2$ is included in Figure SI4.

A better performance was observed in the solar RPR with powdered P25 $TiO_2$ compared to $TiO_2$-kaolin pellets when the pesticide mixture was prepared with UW, achieving a higher TOC removal (≈77%; Table SI2) and the complete degradation of pesticides in only 60–90 min of solar irradiation (Figure SI4). These results were due to the much faster photodegradation of imidacloprid and pyrimethanil, while the degradation kinetics of methomyl was slightly slower (Table SI2), just as it has previously described for the titania-kaolin material. On the other hand, a very low photodegradation of the pesticides and a negligible TOC removal were observed when the E2 real MWWTP effluent matrix was used in the experiment (Table SI2 and Figure SI4). In this case, it was observed that the P25 $TiO_2$ powder was settled on the bottom of the RPR due to the basic pH value of this matrix (pH = 8.1–8.6).

This significantly worse performance of the P25 $TiO_2$ catalyst must be mainly attributed to the strong aggregation of these catalyst particles at high pH values, such as those found in MWWTP effluents (Table 1). In this environment, different ions, including $H^+$ and $HO^-$, can bind to $TiO_2$, changing its surface potential and affecting the photoefficiency of the titania particles (Tolosana-Moranchel et al., 2017). In fact, at basic pH values of 8.1–8.6, far from the isoelectric point of $TiO_2$ ($pH > pH_{IEP}$ = 6.2, for P25 $TiO_2$), the surface of titania particles becomes negatively charged because $TiO^-$ species predominate, favouring their aggregation (Tolosana-Moranchel et al., 2017, 2021). For this reason, titania nanoparticles tend to agglomerate and become larger particles under basic pH conditions. This reduces the available surface area and the active sites for the reaction and generates very high scattering (Tolosana--Moranchel et al., 2020), also causing the catalyst to settle. As a result, there is a significant reduction in the efficiency of this photocatalyst under basic conditions (Ahmed and Haider, 2018; Luna-Sanguino et al., 2021; Li et al., 2010).

On the other hand, although lower TOC removal (61.1%) and slower degradation rates were obtained with the titania-kaolin catalyst in UW compared to those with P25 $TiO_2$, a much better photocatalytic performance of the pellets was found under the effect of the two MWWTPs end-effluents that were tested (E1 and E2, Table 1). In particular, a good

photocatalytic treatment efficiency was obtained in the E1 matrix with the titania-kaolin material, achieving the complete degradation of pesticides (170 min of solar irradiation for pyrimethanil and 280 min for imidacloprid and methomyl) and a TOC removal of 55.7% after 300 min of photocatalytic treatment. In the more complex E2 MWWTP effluent, a slightly lower 53.6% TOC removal was achieved in 300 min, while total pesticide photodegradation required about 300 min of solar irradiation (*ca.* 240 min for pyrimethanil) (Table SI2 and Fig. 6).

It has been reported that the photodegradation of organic pollutants is strongly influenced by the quality and composition of the water matrix to be treated. Thus, the efficiency of a photocatalytic process is influenced by the presence of some dissolved components that can either inhibit or promote the ongoing degradation mechanism (Adams and Impellitteri, 2009; Lado Ribeiro et al., 2019; Muelas-Ramos et al., 2022; Li et al., 2022; Pérez-Lucas et al., 2023). Natural water and wastewater contain a wide range of organic substances (*e.g.*, natural organic matter consisting mainly of humic and fulvic acids, carbohydrates, and proteins) and inorganic species (*e.g.*, $CO_3^{2-}$, $HCO_3^-$, $NO_2^-$, $SO_4^{2-}$, and $Cl^-$) that react with $HO^\bullet$, either competing with the pollutants for their oxidation (Rioja et al., 2016) or forming alternative radicals with lower oxidation potential, resulting in lower process efficiency (Michael et al., 2012). In particular, the presence of high concentrations of inorganic ions (mainly $CO_3^{2-}$, $Cl^-$, $SO_4^{2-}$, and $Ca^{2+}$) in the two effluents used (E1 and E2, Table 1) could represent a limitation for the solar photocatalytic activity of the catalytic pellets (Santiago et al., 2014). In fact, they exert an inhibitory effect on the catalytic activity and can also attenuate the amount of radiation reaching the pellets by means of light absorption. In addition, a high concentration of carbonate species, which can act as $HO^\bullet/h^+$ scavengers, can lead to the formation of less powerful oxidants, such as $CO_3^{\bullet-}$, $NO_3^{\bullet-}$, or $Cl^{\bullet-}$, among others (Klamerth et al., 2009; Zhang et al., 2012).

However, the titania-kaolin catalyst was successful in photodegrading the pesticides under the complex MMWTP effluent matrices (Table SI2), when compared to the performance of other photodegradation processes using $TiO_2$-based powder catalysts. Some commercial $TiO_2$ catalysts (such as Evonik P25, P25/20 and P90) showed poorer activity and significantly lower TOC removal when UW was just replaced by tap water, which is a relatively simple aqueous matrix (Carbajo et al., 2014). Moreover, the effect of the natural water matrix doubled the time required for the complete degradation of several pesticides over titania-reduced graphene oxide nanocomposites (Luna-Sanguino et al., 2021). It should be noted that the use of these nanoparticulate photocatalysts in suspension poses the problem of difficult recovery after treatment, which is not necessary with the pellets used in this study. On the other hand, the studies on the photodegradation of pesticides using immobilized $TiO_2$ catalysts have been carried out in neutral (M'Bra et al., 2019) or slightly acidic aqueous matrices (Kaur et al., 2018; Sraw et al., 2018), which prevents a direct comparison with the results presented here.

Finally, the stability and reusability of the titania-kaolin catalyst pellets were also evaluated under the influence of the E2 effluent for three consecutive solar runs of 300 min each in the solar RPR. The pellets were recovered after each use, cleaned according to the low-cost washing protocol described in the experimental section, and reused. Similar to the UW experiments, a progressive decrease in TOC removal was observed with successive cycles, *i.e.*, TOC removal values of 53.6%, 45.1% and 43.4% were achieved in the first, second and third uses, respectively; which is consistent with the slight decreases in photodegradation rates observed for the three pesticides after each reuse cycle (Fig. 7). Correspondingly, significantly higher photoefficiency losses were observed in this case than would be inferred from the reduction in BET surface area and mesoporosity of the catalytic pellets after three cycles of reuse (Table 5), but a decrease in the concentration of $TiO_2$ available at the surface could account for the difference. This confirms the previously discussed fouling-induced catalytic deactivation described for the UW matrix, but to a greater extent in the case of MWWTP effluents, probably due to the many other substances present in these effluents that can accumulate on the catalyst pellet surface along successive reuse cycles. Again, the development of an improved washing method seems to be necessary to improve the reusability of these pellet-shaped titania-kaolin catalytic macrocomposites.

### 3.4. Identification of reactive species in the solar photodegradation treatment of the pesticides with the pellet-shaped titania-kaolin catalytic macrocomposites

A series of control solar photocatalytic runs were performed in conical solar batch photoreactors in the presence of the following radical scavengers: 100 mM methanol to scavenge $HO^\bullet$ (Li and Hu, 2018; Feng et al., 2013), 10 mM p-benzoquinone to quench ROS generated from conduction band electrons ($e_{CB}^-$) (Bakar and Ribeiro, 2016; Ye et al., 2019), and 5 mM formic acid as a scavenger for photogenerated holes from the valence band ($h^+$) (Shayegan et al., 2018; Kondrakov et al., 2016). The aim was to unambiguously identify the main reactive species driving the photodegradation mechanism of these studied pesticide mix (5 mg $L^{-1}$ of each pesticide) with the evaluated titania-kaolin catalyst (20 g $L^{-1}$). In particular, the transformation of organic compounds on the surface of the catalyst can take place via direct charge transfer (with $e_{CB}^-$ and $h^+$) or via $HO^\bullet$-based reactions (Shayegan et al., 2018; Kondrakov et al., 2016). In this regard, it is also known that the relative contribution of each alternative reaction pathway to the photo-oxidation process strongly depends on the operating conditions,

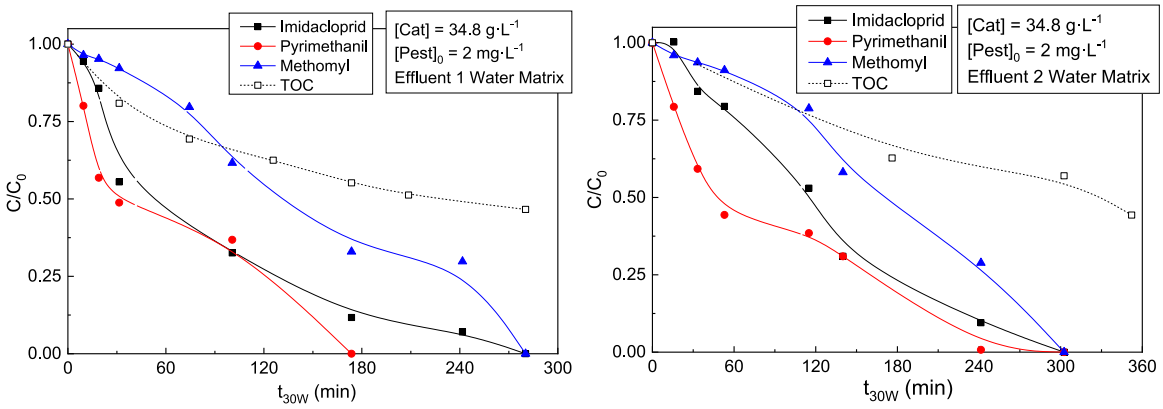


**Fig. 6.** Evolution of pesticide photodegradation in a solar raceway pond reactor under different aqueous matrices: (left) MWWTP Effluent 1 ($pH_0 = 8.0$ and $pH_f = 7.9$), and (right) MWWTP Effluent 2 ($pH_0 = 8.3$ and $pH_f = 8.0$). Imidacloprid (■),pyrimethanil (●), and methomyl (▲), and TOC (□). Operating conditions: [catalyst] = 34.8 g $L^{-1}$, $[pesticides]_0 = 2$ mg $L^{-1}$ of each pesticide in the mixture, $[TOC]_0 = 9$ mg $L^{-1}$.

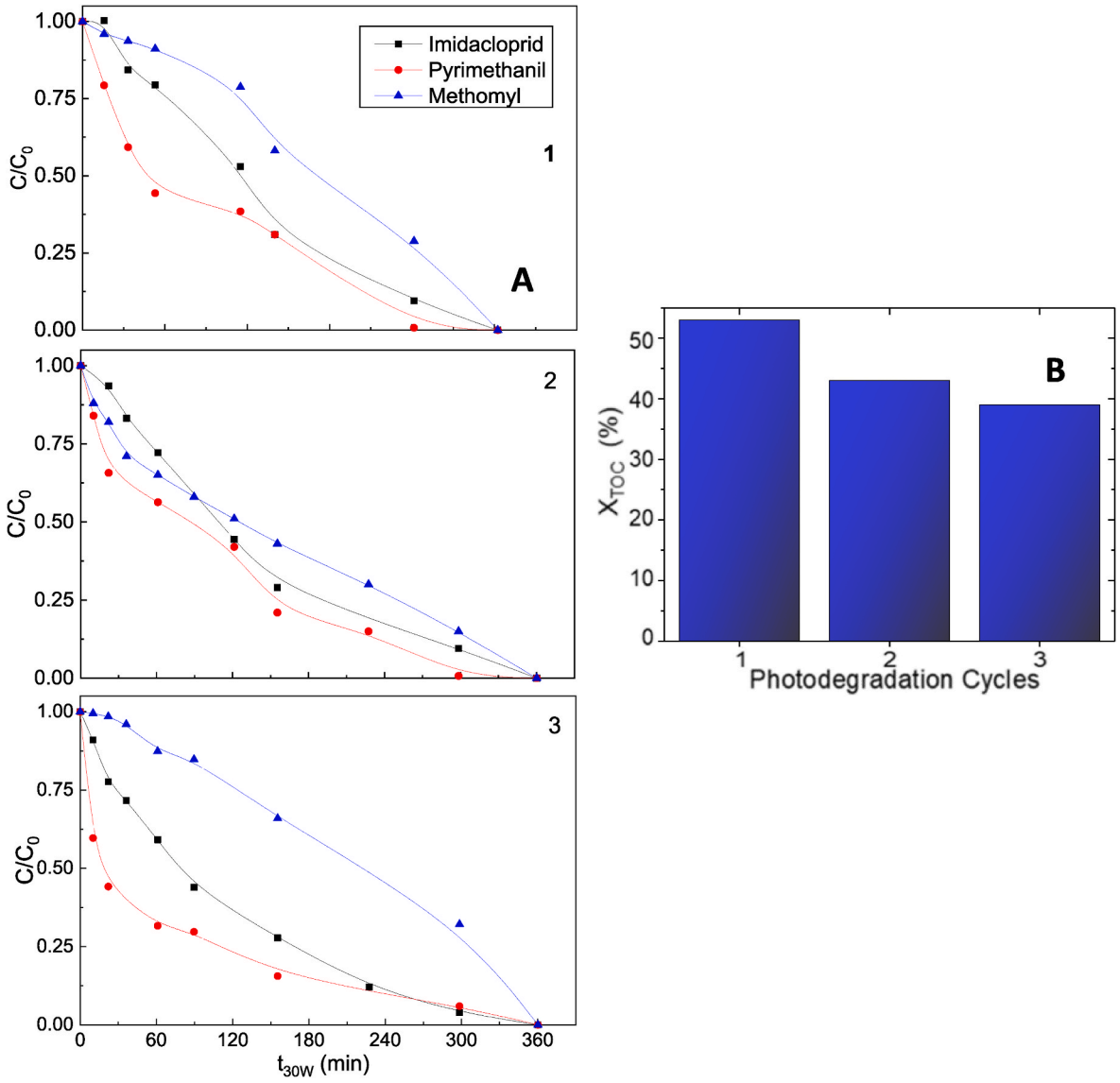


**Fig. 7.** (A) Evolution of pesticides photodegradation and (B) TOC conversion ($X_{TOC}$, %) along three consecutive use cycles (1, 2, 3–300 min each) of the catalytic pellets in a solar raceway pond reactor RPR under MWWTP effluent (E2). Imidacloprid (■),pyrimethanil (●), and methomyl (▲). Operating conditions: [catalyst] = 34.8 g $L^{-1}$, $[pesticides]_0$ = 2 mg $L^{-1}$ of each pesticide in the mixture, $[TOC]_0$ = 9 mg $L^{-1}$, ambient T and P.

the chemical properties of the pollutants, the surface properties of the photocatalysts, and the interaction among these factors (Nafradi et al., 2021). The reduction in the concentration of the three pesticides in the mixture upon their solar photodegradation treatment in the absence and presence of each scavenger using these catalytic pellets in conical solar batch reactors is shown in Fig. 8.

Pyrimethanil and methomyl showed a significant reduction in their photo-oxidation rates in the presence of methanol, while a lesser effect was observed in the case of imidacloprid, which was previously reported to be mainly photodegraded by $HO^{\bullet}$ (Kobkeatthawin et al., 2022), but was not detected here. In fact, it is well known that the generation of $HO^{\bullet}$ can take place via two different pathways: *a)* by oxidation of water molecules on the titania surface via direct charge transfer by $h^+$, and *b)* by different processes involving the hydroperoxyl radicals ($HOO^{\bullet}$) generated from the conduction band electrons ($e^-_{CB}$) (Chen et al., 2005; Cruz-Ortiz et al., 2017; Canle et al., 2012; Romeiro et al., 2018). Thus, to avoid the generation of $HO^{\bullet}$ from water oxidation, formic acid was used to scavenge $h^+$, and different effects were observed for the three pesticides (Fig. 8). A significant decrease in the photo-oxidation rate was observed for pyrimethanil and methomyl, but not as much as with the addition of methanol (Fig. 8). However, the photodegradation of imidacloprid was slightly faster (100% conversion after 240 min of solar irradiation, Fig. 8 and Table SI3). This outcome is probably due to the promotion of $e^-$ from the valence band (VB) to the conduction band (CB) of titania, then formic acid quickly reacts with the holes in the VB and prevents the recombination of the $e^-_{CB}/h^+$ charge carriers, making $e^-_{CB}$ more available to react with imidacloprid, as described in (Tolosana-Moranchel et al., 2018). Finally, when p-benzoquinone was added to quench the ROS formed from $e^-_{CB}$, some inhibition was always observed, especially in the case of pyrimethanil and methomyl, although imidacloprid initially showed a very fast degradation that was then strongly inhibited (Fig. 8 and Table SI3).

Considering the results obtained in these photodegradation studies in the presence of radical scavengers, it is clear that the photo-oxidation of imidacloprid follows a different pathway than that of pyrimethanil and methomyl, indicating that its chemical structure with more functional groups may lead to a complex photodegradation mechanism (Fig. 8 and Table SI3). Therefore, a relatively low contribution of $h^+$ species to the photodegradation of imidacloprid was observed, while the predominant reactive species involved in this mechanism are electrons

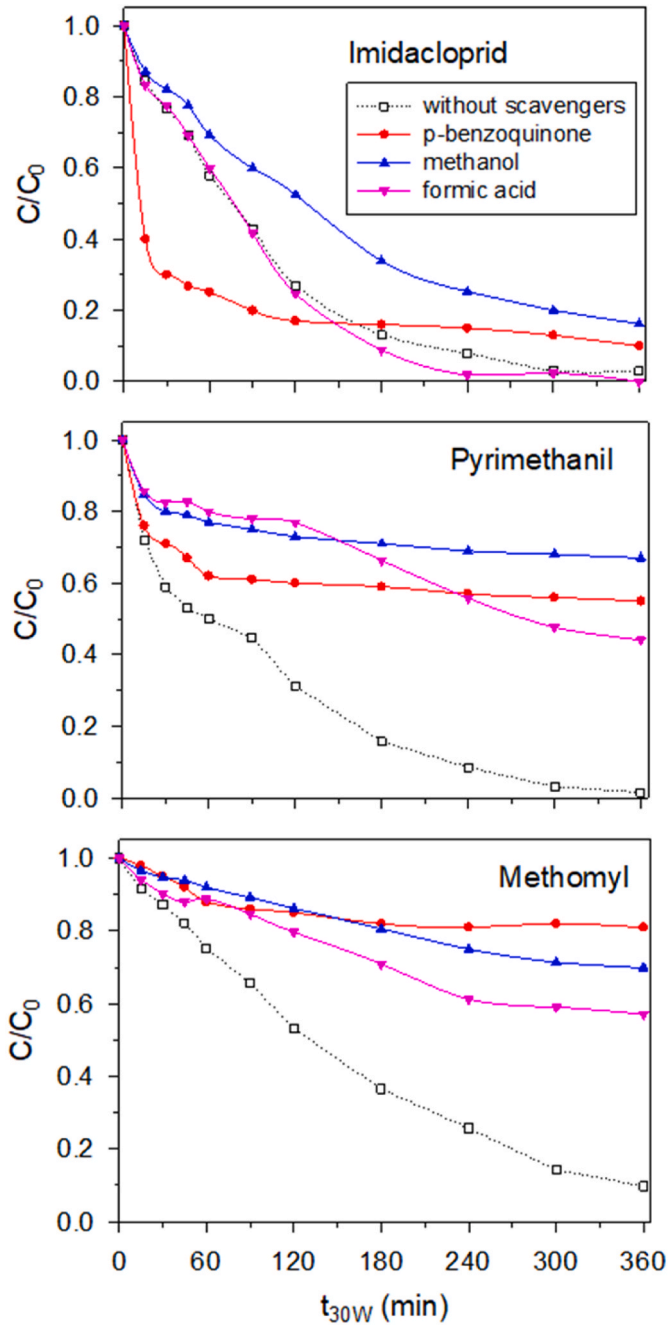


**Fig. 8.** Solar photodegradation of pesticides mix under UW in conical solar batch photoreactors in the absence and presence of radical scavengers. Without scavenger (□) and with p-benzoquinone (●), methanol (▲), and formic acid (▼). Operating conditions: [catalyst] = 20 g $L^{-1}$, $[pesticides]_0$ = 5 mg $L^{-1}$ of each pesticide in the mixture, ambient T and P.

and ROS other than $HO^{\bullet}$. These species play an essential role in the photodegradation of imidacloprid because electrons can react directly with the pollutant. Unlike the other pesticides studied, imidacloprid contains a very polar nitro functional group, which could facilitate its adsorption on the catalyst surface molecule. On the other hand, these results indicate that in the photodegradation of pyrimethanil and methomyl there are contributions from $HO^{\bullet}$, the ROS generated from $e^-_{CB}$ and a pathway involving $h^+$.

The effect of the studied scavengers can be better analyzed from the following ratios (%) between the inhibited kinetic constants and the overall $k$ value. Thus, $k_{CH_3OH}$, $k_{HCOOH}$ and $k_{p-benzoquinone}$ are the pseudo-first order rate constants estimated for the inhibited reactions carried out in the presence of methanol ($CH_3OH$), formic acid (HCOOH) and p-benzoquinone, respectively; and the total $k$ is calculated taking into account all photo-oxidation processes mediated by both holes ($h^+$) and electrons ($e^-_{CB}$), and is obtained from the fastest process in the presence or absence of scavengers (Luna-Sanguino et al., 2019; Pastrana-Martínez et al., 2013; Tolosana-Moranchel et al., 2017). The comparative study of the relative relevance of these kinetic ratios, as described in Table 6, led to the values shown in Fig. 9. In accordance with the previous discussion, the reaction with $e^-_{CB}$ and with other ROS formed from $e^-_{CB}$ was the main pathway involved in the photo-oxidation of imidacloprid, where a minor contribution of direct photodegradation by $h^+$ was also detected. $HO^{\bullet}$ generated from photoinduced $h^+$ was the dominant species photodegrading pyrimethanil and methomyl, with a high contribution factor of 53.6% and 77.0%, respectively (Fig. 9), whereas the remaining degradation must be attributed to $h^+$ and ROS with a similar weight.

## 4. Conclusions

Three pesticides (imidacloprid, pyrimethanil, and methomyl, at a concentration of 2 mg $L^{-1}$ each) were completely photodegraded by solar-assisted heterogeneous photocatalytic treatment in ultrapure water ($t_{30W} < 270$ min), and also in complex water matrices with basic pH values, such as MWWTP effluents ($t_{30W} \leq 300$ min) in a semi-pilot-scale raceway pond reactor using an optimal dosage of pellet-shaped titania-kaolin macrocomposites of 34.8 g $L^{-1}$. Lower TOC removals (≈53–56%) were found under the effect of two complex MWWTP effluents than in ultrapure water (>60%). Methomyl was always the most recalcitrant pesticide in the mixture to solar photodegradation.

The photodegradation mechanism of this selected mixture of pesticides was studied in conical-batch solar photoreactors. In conclusion, $HO^{\bullet}$ generated from photoinduced holes ($h^+$) was the dominant species in the photodegradation of pyrimethanil and methomyl, while ROS formed from conduction band electrons were the main active species involved in the photo-oxidation of imidacloprid.

Finally, the global evaluation of this solar photocatalytic process with titania-kaolin catalytic pellets have provided very promising pesticide photodegradation results compared to the almost negligible TOC removal achieved with the commercial P25 $TiO_2$ powder in the basic MWWTP effluents studied here, due to the strong effect of titania particle aggregation. Therefore, the use of these novel titania-kaolin macrocomposites has led to an improved behaviour in the application of solar photocatalysis to basic wastewater containing pesticide-type pollutants.

## CRediT authorship contribution statement

**K. Jiménez-Bautista:** Methodology, Validation, Investigation, Formal analysis, Data curation. **A. Gascó:** Conceptualization, Validation, Data curation, Supervision, Funding acquisition, Writing – original draft. **D.R. Ramos:** Conceptualization, Software, Visualization, Formal analysis, Data curation, Writing – original draft. **E. Palomo:** Methodology, Validation, Investigation, Data curation, Visualization, Formal analysis. **V. Muelas-Ramos:** Visualization, Validation, Investigation,

**Table 6**
Calculated kinetic ratios to quantify the elucidated mechanism of the photo-oxidation of the three-pesticide mix (imidacloprid, pyrimethanil and methomyl).

| Kinetic ratio contribution (%) | Photo-mechanism |
|---|---|
| $k_1 = (k_{p-benzoquinone} - k_{CH_3OH})/k$ | Oxidation by $HO^{\bullet}$ radicals generated from photoinduced $h^+$ |
| $k_2 = k_{CH_3OH}/k$ | Direct photodegradation by photogenerated holes ($h^+$) |
| $k_3 = k_{HCOOH}/k$ | Photo-oxidation by Reactive Oxygen Species (ROS) generated from $e^-_{CB}$ ($O_2^{\bullet-}$, $HO_2^{\bullet}$, $HO^{\bullet}$) |

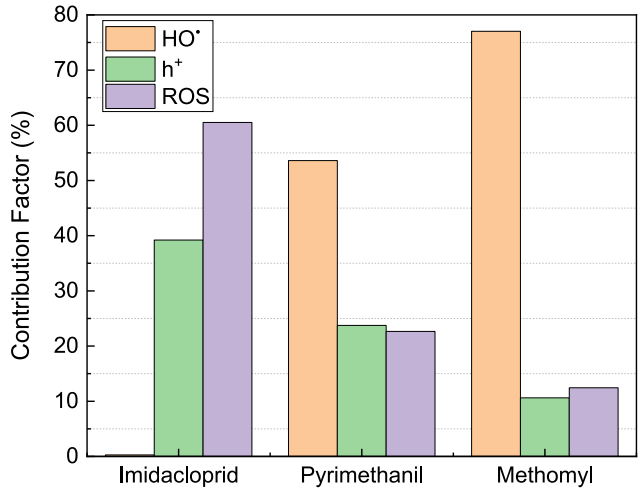


**Fig. 9.** Contribution factor of different reactive species in the photodegradation mechanism of 3 pesticides under solar photocatalytic treatment using the catalytic pellets.

Data curation, Formal analysis, Software. **M. Canle:** Validation, Formal analysis, Data curation, Supervision, Funding acquisition, Writing – original draft. **D. Hermosilla:** Validation, Investigation, Data curation, Supervision, Funding acquisition, Writing – original draft. **A. Bahamonde:** Conceptualization, Data curation, Supervision, Project administration, Funding acquisition, Writing – original draft.

## Declaration of competing interest

The authors declare that they have no known competing financial interests or personal relationships that could have appeared to influence the work reported in this paper.

## Data availability

Data will be made available on request.

## 5. Acknowledgements

This research has been developed in the framework of Projects PID2020-114918RB-I00 (PHOTOPREBIO), funded by MCIN/AEI/10.13039/501100011033, Project PID2021-124021OB-I00 (URBRAIN-TREAT), funded by MCIN/AEI/10.13039/501100011033 and "ERDF: A way of making Europe", and project TED2021-132667B–I00, funded by the EU NextGeneration EU/PRTR through project MCIN/AEI/10.13039/501100011033. M.C. and D.R.R. acknowledge financial support from "*Xunta de Galicia*" (Spain, Project GPC ED431B 2020/52), and D.R.R. acknowledges *Universidade da Coruña* for a *Margarita Salas* contract.

Scanning Electron Microscopy (SEM) analysis were performed at Centro Nacional de Microscopía Electrónica (ICTS – CNME, Universidad Complutense de Madrid, Spain).

## Appendix A. Supplementary data

Supplementary data to this article can be found online at https://doi.org/10.1016/j.jclepro.2023.139203.

## References

Adams, W.A., Impellitteri, C.A., 2009. The photocatalysis of N,N-diethyl-m-toluamide (DEET) using dispersions of Degussa P-25 $TiO_2$ particles. J. Photochem. Photobiol., A: Chem 202 (1), 28–32.

Adan, C., Martinez-Arias, A., Malato, S., Bahamonde, A., 2009. New insights on solar photocatalytic degradation of phenol over Fe-$TiO_2$ catalysts: photo-complex mechanism of iron lixiviates. Appl. Catal. B Environ. 93 (2), 96–105.

Agriculture & Environment Research Unit (AERU), 2023. University of Hertfordshire (UK). Pesticides properties Database. http://sitem.herts.ac.uk/aeru/ppdb/en/index.htm, 09-18-23.

Aguilar, S.D., Ramos, D.R., Santaballa, J.A., Canle, M., 2023a. Preparation, characterization and testing of a bulky non-supported photocatalyst for water pollution abatement. Catal. Today 413–415, 113992.

Aguilar, S., Guerrero, B., Benítez, A., Ramos, D.R., Santaballa, J.A., Canle, M., Rosado, D., Moreno-Andrés, J., 2023b. Inactivation of *E. coli* and *S. aureus* by novel binary clay/semiconductor photocatalytic macrocomposites under UVA and sunlight irradiation. J. Environ. Chem. Eng. 11, 110813.

Ahmed, S.N., Haider, W., 2018. Heterogeneous photocatalysis and its potential applications in water and wastewater treatment: a review. Nanotechnology 29, 342001.

Argly, M.D., Bartholomew, C.H., 2015. Heterogeneous catalyst deactivation and regeneration: a review. Catalyst 5 (1), 145–269.

Bagheri, S., Muhd Julkapli, N., Bee Abd Hamid, S., 2014. Titanium dioxide as a catalyst support in heterogeneous catalysis. Sci. World J. 72749.

Bakar, S.A., Ribeiro, C., 2016. A comparative run for visible-light-driven photocatalytic activity of anionic and cationic S-doped $TiO_2$ photocatalysts: a case study of possible sulfur doping through chemical protocol. J. Mol. Catal. Chem. 421, 1–15.

Barbosa, M.O., Moreira, N.F.F., Ribeiro, A.R., Pereira, M.F.R., Silva, A.M.T., 2016. Occurrence and removal of organic micropollutants: an overview of the watch list of EU Decision 2015/495. Water Res. 94, 257–279.

Borges, M.E., Sierra, M., Cuevas, E., García, R.D., Esparza, P., 2016. Photocatalysis with solar energy: sunlight-responsive photocatalyst based on $TiO_2$ loaded on a natural material for wastewater treatment. Sol. Energy 135, 527–535.

Cabrera-Reina, A., Miralles-Cuevas, S., Soriano-Molina, P., Sánchez-Pérez, J.A., 2021. A critical evaluation of the use of accumulated energy as a parameter for the scale-up of solar photoreactors during the treatment of simulated industrial wastewater by solar photo-Fenton. J. Chem. Technol. Biotechnol. 96, 1593–1602.

Canle, M., Antão-Geraldes, A.M., 2023. A snapshot on the occurrence and risk assessment of organic pollutants in an urban river. Appl. Sci. 13 (1), 146.

Canle, M., Fernández, M.I., Martínez, C., Santaballa, J.A., 2012. (Re)Greening photochemistry: using light for degrading persistent organic pollutants. Rev. Environ. Sci. Biotechnol. 11, 213–221.

Carbajo, J., García-Muñoz, P., Tolosana-Moranchel, A., 2014. Effect of water composition on the photocatalytic removal of pesticides with different $TiO_2$ catalysts. Environ. Sci. Pollut. Res. 21, 12233–12240.

Carra, I., Santos-Juanes, L., Gabriel, F., Fernández, A., Malato, S., Sánchez Pérez, J.A., 2014. New approach to solar photo-Fenton operation. Raceway ponds as tertiary treatment technology. J. Hazard Mater. 279, 322–329.

Chen, Y., Yang, S., Wang, K., Lou, L., 2005. Role of primary active species and $TiO_2$ surface characteristic in UV-illuminated photodegradation of Acid Orange 7. J. Photochem. Photobiol., A: Chem 172, 47–54.

Cruz-Ortiz, B.R., Hamilton, J.W.J., Pablos, C., Diaz-Jiménez, L., Cortes-Hernández, D.A., Sharma, P.K., Castro-Alférez, M., Fernández-Ibáñez, P., Dunlop, P.S.M., Byrne, J.A., 2017. Mechanism of photocatalytic disinfection using titania-graphene composites under UV and visible irradiation. Chem. Eng. J. 316, 179–186.

De la Obra, I., Ponce-Robles, L., Miralles-Cuevas, S., Oller, I., Malato, S., Sánchez Pérez, J.A., 2017. Microcontaminant removal in secondary effluents by solar photo-Fenton at circumneutral pH in raceway pond reactors. Catal. Today 287, 10–14.

Deng, X., Zheng, X., Jia, F., Cao, C., Song, H., Jiang, Y., Liu, Y., Liu, G., Li, S., Wang, L., 2023. Unspecific peroxygenases immobilized on Pd-loaded three-dimensional ordered macroporous (3DOM) titania photocatalyst for photo-enzyme integrated catalysis. Appl. Catal. B Environ. 330, 122622.

Dijkstra, M.F.J., Michorius, A., Buwalda, H., Panneman, H.J., Winkelman, J.G.M., Beenackers, A.A.C.M., 2001. Comparison of the efficiency of immobilized and suspended systems in photocatalytic degradation. Catal. Today 66 (2–4), 487–494.

Evgenidou, E., Ainali, N.M., Rapti, A., Bikiaris, R.D., Nannou, C., Lambropoulou, D.A., 2023. Photocatalytic performance of buoyant $TiO_2$-immobilized poly(ethylene terephthalate) beads for the removal of the anticonvulsant drug pregabalin from water and leachate. J. Environ. Chem. Eng. 11 (5), 110697.

Fantke, P., Gillespies, B.W., Juraske, R., Joillet, O., 2014. Estimating half-lives for pesticide dissipation from plants. Environ. Sci. Technol. 48 (15), 8588–8602.

Feng, H., Tran, T., Chen, L., Yuan, L., Cai, Q., 2013. Visible light-induced efficiently oxidative decomposition of p-nitrophenol by CdTe/$TiO_2$ nanotube arrays. Chem. Eng. J. 215–216, 591–599.

Fiorentino, A., Esteban, B., Garrido-Cárdenas, J.A., Kowalska, K., Rizzo, L., Agüera, A., Sánchez-Pérez, J.A., 2019. Effect of solar photo-Fenton process in raceway pond reactors at neutral pH on antibiotic resistance determinants in secondary treated urban wastewater. J. Hazard Mater. 378, 120737.

García-Muñoz, P., Carbajo, J., Faraldos, M., Bahamonde, A., 2014. Photocatalytic degradation of phenol and isoproturon: effect of adding an activated carbon to titania catalyst. J. Photochem. Photobiol., A: Chem 287, 8–18.

Gaya, U.I., Abdullah, A.H., 2008. Heterogeneous photocatalytic degradation of organic contaminants over titanium dioxide: a review of fundamentals, progress and problems. J. Photochem. Photobiol. C Photochem. Rev. 9, 1–12.

Guillard, C., Disdier, J., Monnet, C., Dussaud, J., Malato, S., Blanco, J., Maldonado, M.I., Herrmann, J.-M., 2003. Solar efficiency of a new deposited titania photocatalyst: chlorophenol, pesticide and dye removal applications. Appl. Catal., B 46, 319–332.

Hanaor, D.A.H., Sorrell, C.C., 2011. Review of the anatase to rutile phase transformation. J. Mater. Sci. 46 (4), 855–874.

Hermosilla, D., Cortijo, M., Huang, C.P., 2009. The role of iron on the degradation and mineralization of organic compounds using conventional Fenton and photo-Fenton processes. Chem. Eng. J. 155 (3), 637–646.
Ibhadon, A.O., Fitzpatrick, P., 2013. Heterogeneous photocatalysis: recent advances and applications. Catalysts 3 (1), 189–218.
Jenkins, R., Zinder, R.L., 1996. Introduction to X-Ray Powder Diffractometry. John Wiley & Sons Inc., New York, p. 9.
Jiménez-Tototzintle, M., Oller, I., Hernández-Ramírez, A., Malato, S., Maldonado, M.I., 2015. Remediation of agro-food industry effluents by biotreatment combined with supported $TiO_2/H_2O_2$ solar photocatalysis. Chem. Eng. J. 273, 205–213.
Jin, L., Xie, J., Wong, C.K.C., Chan, S.K.Y., Abbaszade, G., Schnelle-Kreis, J., Zimmermann, R., Li, J., Zhang, G., Fu, P., Li, X., 2019. Contributions of city-specific fine particulate matter ($PM_{2.5}$) to differential *in vitro* oxidative stress and toxicity implications between Beijing and Guangzhou of China. Environ. Sci. Technol. 53 (5), 2881–2891.
Kaur, T., Sraw, A., Wanchoo, R.K., Toor, A.P., 2018. Solar assisted degradation of carbendazim in water using clay beads immobilized with $TiO_2$ & Fe doped $TiO_2$. Sol. Energy 162, 45–56.
Klamerth, N., Miranda, N., Malato, S., Agüera, A., Fernández-Alba, A.R., Maldonado, M. I., Coronado, J.M., 2009. Degradation of emerging contaminants at low concentrations in MWTPs effluents with mild solar photo-Fenton and $TiO_2$. Catal. Today 144 (1–2), 124–130.
Kobkeatthawin, T., Trakulmututa, J., Amornsakchai, T., Kajitvichyanukul, P., Smith, S. M., 2022. Identification of active species in photodegradation of aqueous imidacloprid over g-$C_3N_4$/$TiO_2$ nanocomposites. Catalysts 12, 120.
Kondrakov, A.O., Ignatev, A.N., Lunin, V.V., Frimmel, F.H., Bräse, S., Horn, H., 2016. Roles of water and dissolved oxygen in photocatalytic generation of free OH radicals in aqueous $TiO_2$ suspensions: an isotope labeling study. Appl. Catal., B 182, 424–430.
Kumar, S.G., Devi, L.G., 2011. Review on modified $TiO_2$ photocatalysis under UV visible light. J. Phys. Chem. A 115 (46), 13211–13241.
Kusworo, T.D., Budiyono, B., Kumoro, A.C., Utomo, D.P., 2022. Photocatalytic nanohybrid membranes for highly efficient wastewater treatment: a comprehensive review. J. Environ. Manag. 137, 115357.
Lado Ribeiro, A.R., Noreira, N.F.F., Puma, G.L., Silva, A.M.T., 2019. Impact of water matrix on the removal of micropollutants by advanced oxidation technologies. Chem. Eng. J. 363, 155–173.
Li, S., Hu, J., 2018. Transformation products formation of ciprofloxacin in UVA/LED and UVA/LED/$TiO_2$ systems: impact of natural organic matter characteristics. Water Res. 132, 320–330.
Li, G., Lv, L., Fan, H., Ma, J., Li, Y., Wan, Y., Zhao, X.S., 2010. Effect of the agglomeration of $TiO_2$ nanoparticles on their photocatalytic performance in the aqueous phase. J. Colloid Interface Sci. 348 (2), 342–347.
Li, J., Fei, L., Li, S., Xue, C., Shi, Z., Hinkelmann, R., 2020. Development of "water-suitable" agriculture based on a statistical analysis of factors affecting irrigation water demand. Sci. Total Environ. 744, 140986.
Li, D., Feng, Z., Zhou, B., Chen, H., Yuan, R., 2022. Impact of water matrices on oxidation effects and mechanisms of pharmaceuticals by ultraviolet-based advanced oxidation technologies: a review. Sci. Total Environ. 844, 157162.
Luna-Sanguino, G., Tolosana-Moranchel, A., Duran-Valle, C., Faraldos, M., Bahamonde, A., 2019. Optimized P25-rGO composites for pesticides degradation: elucidation of photo-mechanism. Catal. Today 328, 172–177.
Luna-Sanguino, G., Ruíz-Delgado, A., Duran-Valle, C.J., Malato, S., Faraldos, M., Bahamonde, A., 2021. Impact of water matrix and oxidant agent on the solar assisted photodegradation of a complex mix of pesticides over titania-reduced graphene oxide nanocomposites. Catal. Today 380, 114–124.
Malato, S., Fernández-Ibáñez, P., Maldonado, M.I., Blanco, J., Gernjak, W., 2009. Decontamination and disinfection of water by solar photocatalysis: recent overview and trends. Catal. Today 147 (1), 1–59.
Malato Rodríguez, S., Blanco Gálvez, J., Maldonado Rubio, M.I., Fernández Ibáñez, P., Alarcón Padilla, D., Collares Pereira, M., Farinha Mendes, J., Correia de Oliveira, J., 2004. Engineering of solar photocatalytic collectors. Sol. Energy 77, 513–524.
Michael, I., Hapeshi, E., Osorio, V., Perez, S., Petrovic, M., Zapata, A., Malato, S., Barcelo, D., Fatta-Kassinos, D., 2012. Solar photocatalytic treatment of trimethoprim in four environmental matrices at a pilot scale: transformation products and ecotoxicity evaluation. Sci. Total Environ. 430, 167–173.
Misawa, K., Sekine, Y., Kusukubo, Y., Sohara, K., 2020. Photocatalytic degradation of atmospheric fine particulate matter ($PM_{2.5}$) collected on $TiO_2$ supporting quartz fibre filter. Environ. Technol. 41 (10), 1266–1274.
Muelas-Ramos, V., Sampaio, M.J., Silva, C.G., Bedia, J., Rodriguez, J.J., Faria, J.L., Belver, C., 2021. Degradation of diclofenac in water under LED irradiation using combined g-$C_3N_4$/$NH_2$-MIL-125 photocatalysts. J. Hazard Mater. 416, 126199.
Muelas-Ramos, V., Peñas-Garzón, M., Rodriguez, J.J., Bedia, J., Belver, C., 2022. Solar photocatalytic degradation of emerging contaminants using $NH_2$-MIL-125 grafted by heterocycles. Sep. Purif. Technol. 297, 121442.
M'Bra, I.C., García-Muñoz, P., Drogui, P., Keller, N., Trokourey, A., Didier Robert, D., 2019. Heterogeneous photodegradation of Pyrimethanil and its commercial formulation with $TiO_2$ immobilized on SiC foams. J. Photochem. Photobiol., A: Chem 368, 1–6.
Nafradi, M., Hlogyik, T., Farkas, L., Alapi, T., 2021. Comparison of the heterogeneous photocatalysis of imidacloprid and thiacloprid - reaction mechanism, ecotoxicity, and the effect of matrices. J. Environ. Chem. Eng. 9, 106684.
Nitoi, I., Oncescu, T., Oancea, P., 2013. Mechanism and kinetic study for the degradation of lindane by photo-Fenton process. J. Ind. Eng. Chem. 19, 305–309.
Park, M., Ko, Y.T., Ji, M., Cho, J.S., Wang, D.H., Lee, Y.-I., 2022. Facile self-assembly-based fabrication of a polyvinylidene fluoride nanofiber membrane with immobilized titanium dioxide nanoparticles for dye wastewater treatment. J. Clean. Prod. 378, 134506.
Pastrana-Martínez, L.M., Morales-Torres, S., Kontos, A.G., Moustakas, N.G., Faria, J.L., Doña-Rodríguez, J.M., Falaras, P., Silva, A.M.T., 2013. $TiO_2$, surface modified $TiO_2$, and graphene oxide-$TiO_2$ photocatalysts for degradation of water pollutants under near-UV/Vis and visible light. Chem. Eng. J. 224, 17–23.
Pérez-Lucas, G., Aatik, A.E., Aliste, M., Navarro, G., Fenoll, J., Navarro, S., 2023. Removal of contaminants of emerging concern from a wastewater effluent by solar-driven heterogeneous photocatalysis: a case study of pharmaceuticals. Water Air Soil Pollut. 234, 55.
Pignatello, J.J., Oliveros, E., MacKay, A.A., 2006. Advanced oxidation processes for organic contaminant destruction based on the fenton reaction and related chemistry. Crit. Rev. Environ. Sci. Technol. 36, 1–84.
Prieto-Rodriguez, L., Miralles-Cuevas, S., Oller, I., Agüera, A., Puma, G.L., Malato, S., 2012. Treatment of emerging contaminants in wastewater treatment plants (WWTP) effluents by solar photocatalysis using low $TiO_2$ concentrations. J. Hazard Mater. 211–212, 131–137.
Rahman, M.M., Shafiullah, A.Z., Pal, A., Islam, M.A., Jahan, I., Saha, B.B., 2021. Study on optimum IUPAC adsorption isotherm models employing sensitivity of parameters for rigorous adsorption system performance evaluation. Energies 14, 7478.
Ramos, D.R., Canle, M., Santaballa, J.A., Aguilar, S., 2020. Elemento fotocatalizador para descontaminación de fluidos. Spanish Patent No. ES2916381, PCT application No. ES2021/070940.
Ramos, D.R., Iazykov, M., Fernandez, M.I., Santaballa, J.A., Canle, M., 2021. Mechanical stability is key for large-scale implementation of photocatalytic surface-attached film technologies in water treatment. Front. Chem. Eng. 3, 688498.
Razak, S., Nawi, M.A., Haitham, K., 2014. Fabrication, characterization and application of a reusable immobilized $TiO_2$-PANI photocatalyst plate for the removal of reactive red 4 dye. Appl. Surf. Sci. 319, 90–98.
Ren, L., Huo, W., Li, G., Choi, W., An, T., 2023. Photocatalytic mechanisms and photocatalyst deactivation during the degradation of 5-fluorouracil in water. Catal. Today 410, 45–55.
Rioja, N., Zorita, S., Peñas, F.J., 2016. Effect of water matrix on photocatalytic degradation and general kinetic modeling. Appl. Catal., B 180, 330–335.
Romeiro, A., Azenha, M.E., Canle, M., Rodrigues, V.H.N., Da Silva, J.P., Burrows, H.D., 2018. Titanium dioxide nanoparticle photocatalysed degradation of ibuprofen and naproxen in water: competing hydroxyl radical attack and oxidative decarboxylation by semiconductor holes. ChemistrySelect 3, 10915–10924.
Sánchez, M., 2021. Sistema combinado dixestor-humidal seguido de fotodegradación para a depuración de augas residuais e contaminantes orgánicos emerxentes. Universidade da Coruña, A Coruña, Spain (PhD thesis). http://hdl. handle.net/2183/29365. (Accessed 27 July 2023).
Sánchez, M., Ramos, D.R., Fernández, M.I., Aguilar, S., Ruiz, I., Canle, M., Soto, M., 2022. Removal of emerging pollutants by a 3-step system: hybrid digester, vertical flow constructed wetland and photodegradation post-treatments. Sci. Total Environ. 842, 156750.
Sánchez, M., Fernández, M.I., Ruiz, I., Canle, M., Soto, M., 2023. Combining constructed wetlands and UV photolysis for the advanced removal of organic matter, nitrogen, and emerging pollutants from wastewater. Environments 10 (3), 5.
Santiago, D.E., Araña, J., González-Díaz, O., Alemán-Domínguez, M.E., Acosta-Dacal, A. C., Fernández-Rodríguez, C., Pérez-Peña, J., Doña-Rodríguez, J.M., 2014. Effect of inorganic ions on the photocatalytic treatment of agro-industrial wastewaters containing imazalil. Appl. Catal., B 156–157, 284–292.
Shayegan, Z., Lee, C.S., Haghighat, F., 2018. $TiO_2$ photocatalyst for removal of volatile organic compounds in gas phase - a review. Chem. Eng. J. 334, 2408–2439.
Silva, M.J., Alves, P., Gomes, J., Martins, R.C., Ferreira, P., 2023. Optimization of P25/PDMS supported catalysts preparation for the photocatalytic oxidation of parabens. J. Environ. Chem. Eng. 11 (5), 110610.
Soriano-Molina, P., Plaza-Bolaños, P., Lorenzo, A., Agüera, A., García Sánchez, J.L., Malato, S., Sánchez Pérez, J.A., 2019. Assessment of solar raceway pond reactor for removal contaminants of emerging concern by photo-Fenton at circumneutral pH from very different municipal wastewater effluents. Chem. Eng. J. 366, 141–149.
Spurr, R.A., Myers, H., 1957. Quantitative analysis of anatase-rutile mixtures with an X-ray diffractometer. Anal. Chem. 29, 760–762.
Sraw, A., Kaur, T., Pandey, Y., Sobti, A., Wanchoo, R.K., Toor, A.P., 2018. Fixed bed recirculation type photocatalytic reactor with $TiO_2$ immobilized clay beads for the degradation of pesticide polluted water. J. Environ. Chem. Eng. 6, 7035–7043.
Sun, L., Schindler, K.M., Hoy, A.R., Bolton, J.R., Helz, G.R., Zepp, R.G., Crosby, D.G. (Eds.), 1994. Aquatic and Surface Photochemistry. Lewis Publishers, Boca Ratón, p. 409.
Teixeira, S., Martins, P.M., Lanceros-Méndez, S., Kühn, K., Cuniberti, G., 2016. Reusability of photocatalytic $TiO_2$ and ZnO nanoparticles immobilized in poly (vinylidene difluoride)-co-trifluoroethylene. Appl. Surf. Sci. 384, 497–504.
Toepfer, B., Gora, A., Puma, G.L., 2006. Photocatalytic oxidation of multicomponent solutions of herbicides: reaction kinetics analysis with explicit photon absorption effects. Appl. Catal. B Environ. 68 (3–4), 171–180.
Tolosana-Moranchel, A., Carbajo, J., Faraldos, M., Bahamonde, A., 2017. Solar-assisted photodegradation of isoproturon over easily recoverable titania catalysts. Environ. Sci. Pollut. Res. 24, 7821–7828.
Tolosana-Moranchel, A., Montejano, A., Casas, J.A., Bahamonde, A., 2018. Elucidation of the photocatalytic-mechanism of phenolic compounds. J. Environ. Chem. Eng. 6, 5712–5719.
Tolosana-Moranchel, A., Canle, M., Faraldos, M., Bahamonde, A., 2020. Photo-mechanism of phenolic pollutants in natural water: effect of salts. Sep. Purif. Technol., 11868

Tolosana-Moranchel, A., Pecharromán, C., Faraldos, M., Bahamonde, A., 2021. Strong effect of light scattering by distribution of $TiO_2$ particle aggregates on photocatalytic efficiency in aqueous suspensions. Chem. Eng. J. 403, 126186.

Topalov, A., Abramović, B., Molnár-Gábor, D., Csanádi, J., Arcson, O., 2001. Photocatalytic oxidation of the herbicide (4-chloro-2-methylphenoxy) acetic acid (MCPA) over $TiO_2$. J. Photochem. Photobiol., A: Chem 140 (3), 249–253.

United Nations, Unwater, https://www.unwater.org/water-facts/human-rights-water-and-sanitation, last access September-25-2023..

Villajos, B., Tolosana-Moranchel, A., Canle, M., Farina, A., Gascó, A., Mesa-Medina, S., Faraldos, M., Hermosilla, D., Bahamonde, A., 2021. Photocatalytic degradation of alachlor over titania-reduced graphene oxide nanocomposite: intrinsic kinetic model and reaction pathways. Ind. Eng. Chem. Process Des. Dev. 60 (51), 18907–18917.

Ye, T., Qi, W., An, X., Liu, H., Qu, J., 2019. Faceted $TiO_2$ photocatalytic degradation of anthraquinone in aquatic solution under solar irradiation. Sci. Total Environ. 688, 592–599.

Zhang, W., Li, Y., Su, Y., Mao, K., Wang, Q., 2012. Effect of water composition on $TiO_2$ photocatalytic removal of endocrine disrupting compounds (EDCs) and estrogenic activity from secondary effluent. J. Hazard Mater. 215–216, 252–258.

Zhu, J.L., Chen, S.-P., Lin, W., Huang, H.-D., Li, Z.-M., 2023. Cellulose mineralization with in-situ synthesized amorphous titanium dioxide for enhanced adsorption and auto-accelerating photocatalysis on water pollutant. Chem. Eng. J. 456, 141036.